Grid Forming Converters in Renewable Energy Sources Dominated Power Grid: Control Strategy, Stability, Application, and Challenges

Haobo Zhang, Wang Xiang, Weixing Lin, and Jinyu Wen

***Abstract*—The renewable energy sources (RESs) dominated power grid is an envisaged infrastructure of the future power system, where the commonly used grid following (GFL) control for grid-tied converters suffers from lacking grid support capability, low stability, etc. Recently, emerging grid forming (GFM) control methods have been proposed to improve the dynamic performance and stability of grid-tied converters. This paper reviews existing GFM control methods for the grid-tied converters and compares them in terms of control structure, grid support capability, fault current limiting, and stability. Considering the impact of fault current limiting strategies, a comprehensive transient stability analysis is provided. In addition, this paper explores the typical applications of GFM converters, such as AC microgrid and offshore wind farm high-voltage direct current (OWF-HVDC) integration systems. Finally, the challenges to the GFM converters in future applications are discussed.**

***Index Terms*—Grid following (GFL) control, grid forming (GFM) control, high-voltage direct current (HVDC), microgrid, renewable energy, small-signal stability, transient stability.**

I. Introduction

HIGH penetration of renewable energy sources (RESs), e.g., wind power and photovoltaic solar, has gained increasing attention in recent years to deal with the climate change problem and pave ways to build a carbon-neutral society [1]-[3]. The RESs are integrated into the power grid via grid-tied converters, changing the characteristics of the conventional power grid [4]-[6]. The grid-tied converters of RESs commonly adopt the grid following (GFL) control, which consists of the phase-locked loop (PLL) for synchronization and the vector current control for power control. Due to the lack of grid support capability, the GFL converter behaves like a negative load. With the increasing penetration of converter-interfaced RESs, the conventional synchronous generator (SG) dominated power grid is being changed to a weak power grid with low inertia. Under this condition, a small perturbation will cause large fluctuation and deviation of grid frequency, resulting in low-frequency demand disconnection and even the collapse of the power grid [7]-[9].

To improve the frequency response, enhanced GFL control methods such as current-controlled droop control [10] and current-controlled virtual synchronous generator (VSG) control [11] are proposed to support the power grid. However, when integrating with weak power grids, the GFL control methods will deteriorate the stability of grid-tied converters and induce wide-band frequency oscillation problems. In some practical projects, the frequency oscillation issues already occurred, such as the 1271 Hz oscillation in Lu-Xi high-voltage direct current (HVDC) project [12] and the 20-34 Hz oscillation in Ha-Mi wind farm integration project [13] in China. Moreover, these enhanced GFL control methods still behave like current sources without stand-alone operation capability.

Considering the issues of GFL control in RESs dominated grid, the grid forming (GFM) control is proposed to provide grid support capability. The GFM control is initially designed as constant voltage/frequency (VF) control, which operates as an ideal voltage source to form the AC voltage autonomously. Due to the constant output voltage and frequency, the GFM converter can only integrate with passive power grids (without SGs or GFM converters) [14]. When integrating with active power grids (e.g., SGs and GFM converters), the power synchronization loop (PSL) is added to the VF control to share power among other voltage sources [15]-[24]. The fundamental idea behind this PSL-based GFM control lies in the emulation of the rotor characteristics of SGs, which enable RESs to self-synchronize with power grids without PLL, share power among different power sources, and provide grid support to improve frequency response. Thus, it can overcome the drawbacks of GFL control. In addition to the PSL-based GFM control, a novel virtual oscillator controller (VOC) has been recently proposed as an emerging GFM control [25]. Different from the PSL-based GFM control, the VOC-based GFM control is used to emulate the dynamics of the weak nonlinear limit-cycle oscilla-

Manuscript received: April 25, 2021; accepted: October 25, 2021. Date of CrossCheck: October 25, 2021. Date of online publication: November 30, 2021.

This work was supported by the Xinjiang Autonomous Region Key R&D Projects (No. 2020B02002).

H. Zhang, W. Xiang (corresponding author), and J. Wen are with the State Key Laboratory of Advanced Electromagnetic Engineering and Technology, Huazhong University of Science and Technology, Wuhan 430074, China, and W. Xiang is also with the Department of Electronic and Electrical Engineering, University of Strathclyde, G1 1XW, Glasgow, UK (e-mail: zhanghaobo9902@foxmail.com; xiangwang1003@foxmail.com; jinyu.wen@hust.edu.cn).

W. Lin is with TBEA Sunoasis Company Ltd., Ürümqi 830011, China, and he is also with the State Key Laboratory of Advanced Electromagnetic Engineering and Technology, Huazhong University of Science and Technology, Wuhan 430074, China (e-mail: weixinglin@foxmail.com).

DOI: 10.35833/MPCE.2021.000257

tor. Benefiting from the synchronization characteristic of the coupled oscillator network, the VOC converters can quickly synchronize with each other and reach steady states under any initial conditions [26].

Despite the mentioned grid-friendly merits, the GFM converters may suffer from small-signal stability issues when subjected to grid disturbances in strong active grids [27]-[29]. Additionally, during AC faults, the AC fault current limiting strategies may cause transient instability issues of GFM converters [30]-[32]. The reason is once the fault current exceeds the pre-defined current limiter thresholds, the saturated current will force GFM converters to work in constant current source mode, which affects the power-angle curve and causes transient instability problems.

Aiming at investigating the GFM control for future RESs dominated grid, this paper carries out the overview of the state-of-the-art of GFM control with a focus on control structures, AC fault current limiting capability, stability, application prospects, and future challenges. The outline of this paper is organized as shown in Fig. 1. The drawbacks of common GFL control methods are firstly introduced in Section II. Then, more than 9 types of GFM control methods are introduced in Section III in terms of control structures and operating principles. In Sections IV and V, the AC fault current limiting strategies and stability issues of the GFM converters are analyzed. Especially, the impact of current limiting strategies on transient stability is considered. In Section VI, typical application scenarios of the GFM control methods are explored and highlighted. Finally, key challenges of the GFM control in future applications are envisioned in Section VII, and the conclusion is drawn in Section VIII.

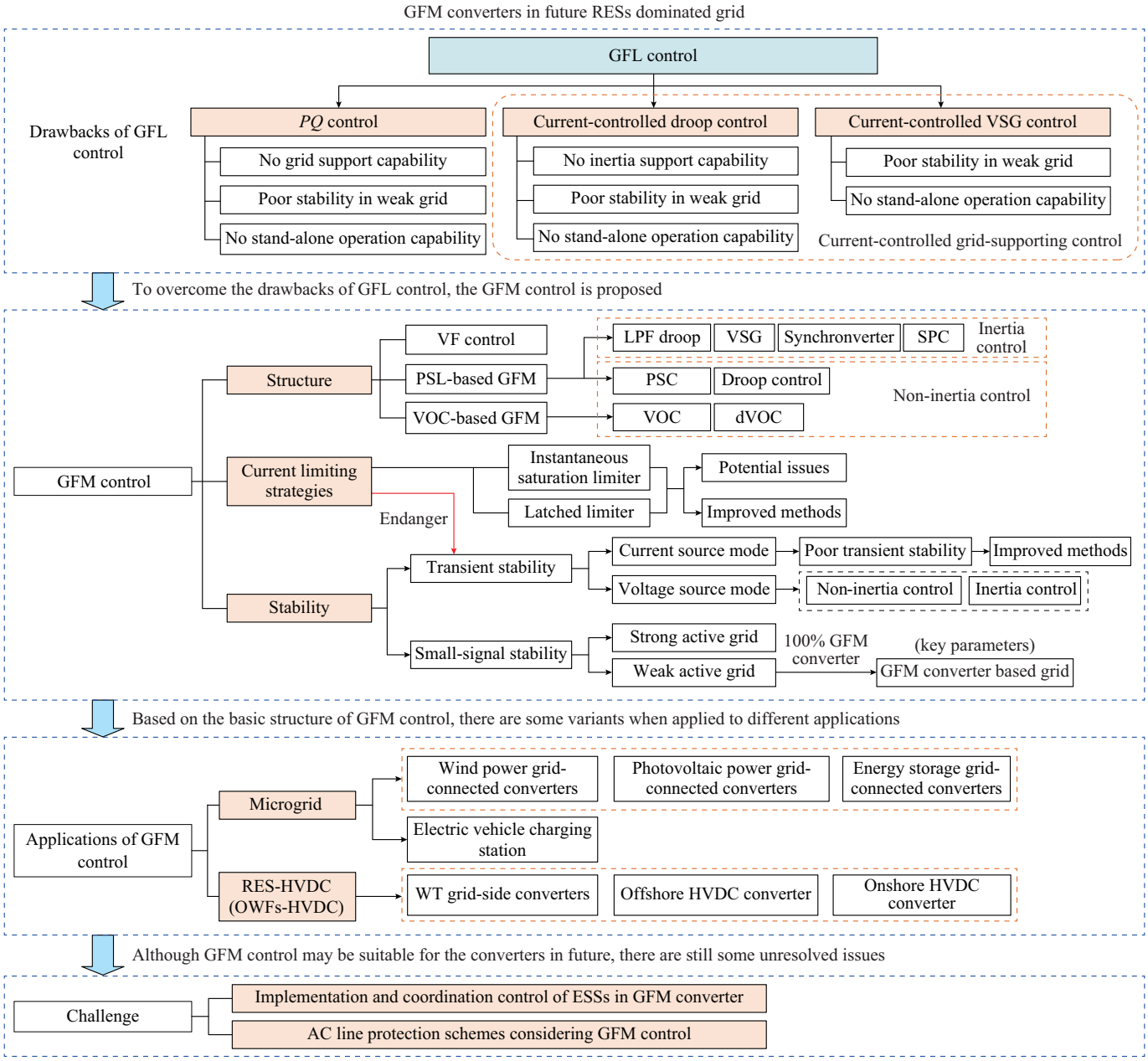

Fig. 1. Overall framework of this paper.

II. GFL Control

A. Active and Reactive Power Control

Typical GFL control consists of the PLL for synchronizing with the power grid and the vector current control for regulating output power. Reference [15] provides the equivalent structure of the GFL converter, which behaves as a controlled current source parallel with an impedance Z, as depicted in Fig. 2 [15], where C_P denotes the outer power control loop (including active power P and reactive power Q); the superscript "*" means the corresponding reference value; and V_1 is the grid-side voltage.

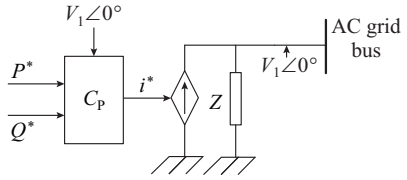

Fig. 2. Equivalent structure of GFL converter.

The common GFL control is the active and reactive power (PQ) control using the proportional-integral (PI) controller, which is shown in Fig. 3 [15], where L and C are the filter inductor and capacitor, respectively; ω_0 is the nominal frequency; V_2 is the modulation voltage of converter; δ is the power angle; and subscripts d and q represent the d- and q-axis values, respectively. Since the power references P^* and Q^* are constant, the PQ-controlled converter has no grid regulation capacity. That may induce a large grid frequency deviation even under a small disturbance [17]. Moreover, since the dynamic of PLL affects the converter output impedance, the PQ-controlled converter has a poor small-signal stability with integration into weak grid, e.g., RESs dominated power grid [33] - [35]. Besides, constrained by controlled current source characteristic, the PQ-controlled converter is a negative load to power grids, which can only transmit power in the presence of a stable AC voltage.

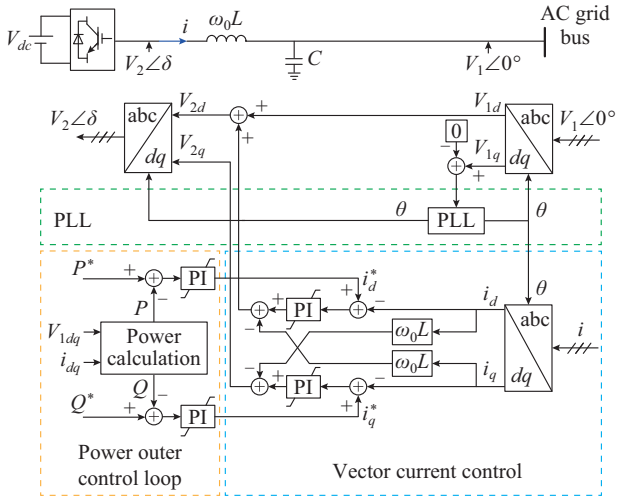

Fig. 3. Structure of typical GFL PQ control.

B. Grid-supporting GFL Control

To improve the frequency response under grid disturbances, there are two grid-supporting GFL control methods that can provide VF support or inertia support for power grids. One is current-controlled droop control, which is depicted in Fig. 4 [10], where m and n are the droop coefficients, and subscripts "0" denote the nominal values.

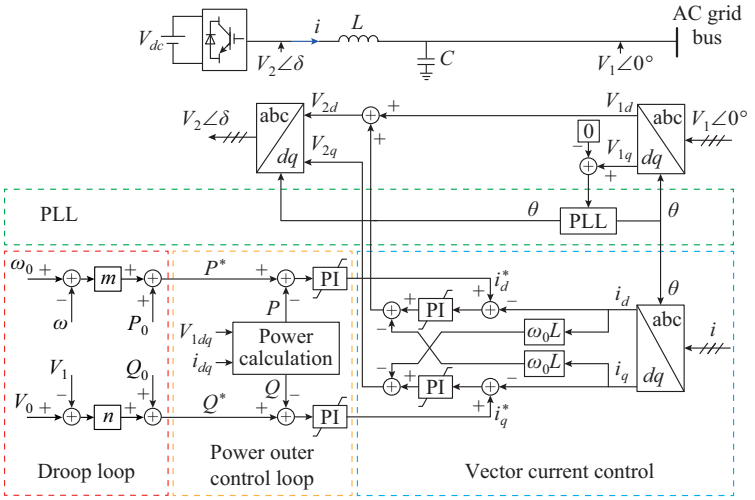

Fig. 4. Structure of current-controlled droop control.

Compared with PQ control, a droop loop is added to regulate the output power. Hence, the converter can respond to grid disturbances, and has grid frequency/voltage regulation capability like SGs. However, this control cannot provide inertia support for the power grid.

The other is the current-controlled VSG control, which aims to provide inertia support for power grids [11]. The structure of the current-controlled VSG control is shown in Fig. 5. Its virtual inertia control is designed referring to the rotor swing equation of SG:

$$J\frac{\mathrm{d}\omega}{\mathrm{d}t}=T_m-T_e-D_P\left(\omega-\omega_0\right)\approx\frac{P_m}{\omega_0}-\frac{P_e}{\omega_0}-D_P\left(\omega-\omega_0\right) \quad (1)$$

where ω is the converter output frequency; P_m and P_e are the mechanical power and electromagnetic power of the SG, respectively; T_m and T_e are the mechanical torque and elec-

tromagnetic torque of the SG, respectively; J is the moment of inertia of the rotor; and D_P is the damping coefficient of SG. At the initial stable state, $P_m = P_e = P_0$, and P_0 is the nominal power. Assuming P_m maintains constant, (1) can be expressed as:

$$\underbrace{\omega_0 J\dot{\omega}}_{\Delta P_i} + \underbrace{\omega_0 D_P\left(\omega-\omega_0\right)}_{\Delta P_d} = P_0 - P_e = -\Delta P_e \tag{2}$$

Equation (2) reflects the dynamic characteristic of SG between electromagnetic power variation ΔP_e and output frequency ω, including the inertia term (the first term ΔP_i) and the damping term (the second term ΔP_d). To imitate this dynamic characteristic utilizing converter control, the power variation ΔP_e is added to the nominal power P_0 to regulate the output power of the converter, as shown in Fig. 5 [11].

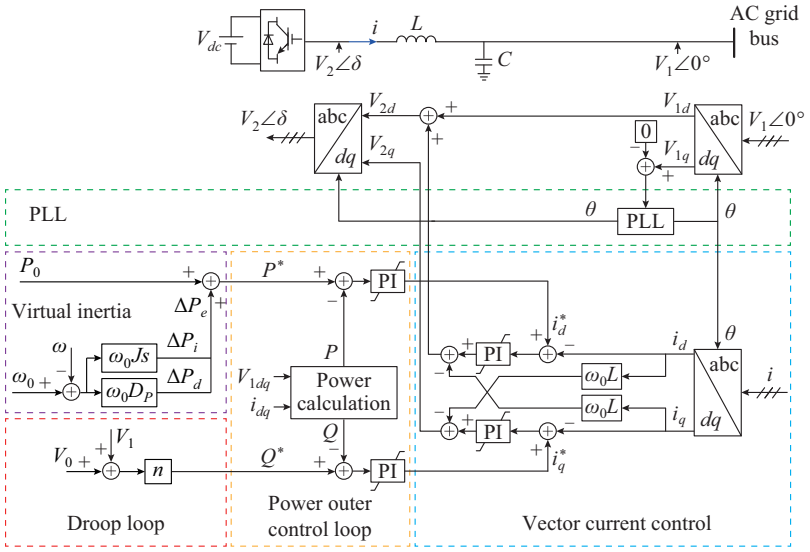

Fig. 5. Structure of current-controlled VSG control.

Although some improvements have been implemented, the inner control of the grid-supporting GFL control methods is still unchanged. Thus, those enhanced methods still operate as the controlled current sources without stand-alone operation capability. In addition, the inherent stability issue caused by PLL in RESs dominated grid is still a potential risk [36].

III. GFM Control

Intrinsically different from GFL converter, GFM converter is a controlled voltage source with the ability to generate AC voltage autonomously [37]. Thus, the GFM control commonly has a voltage control loop and a frequency control loop. Considering different control structures, existing GFM control methods can be divided into three categories: the VF control, the PSL-based GFM control, and the VOC.

A. VF Control

VF control is designed to maintain the output voltage amplitude and frequency constant through the closed-loop control, which is often applied in passive power grids, such as islanded grids or uninterruptable power supply (UPS) systems. However, due to the constant voltage source characteristic, VF-controlled converter has no power-sharing capability, which cannot operate in active power grids.

As shown in Fig. 6 [38], the VF control can be equivalent to a controlled voltage source in series with an output impedance Z, where V represents the output voltage; and C_V is the voltage control loop. In addition, the VF control can be realized through a single-loop control or a dual-loop control. For the single-loop control, the converter output voltage V_{inv}^* is generated directly by the frequency reference value ω^* and reference value of voltage amplitude V^*. While for the dual-loop control, V_{inv}^* is obtained from cascaded voltage and current loops. Thus, the dual-loop control also has the current limiting capability.

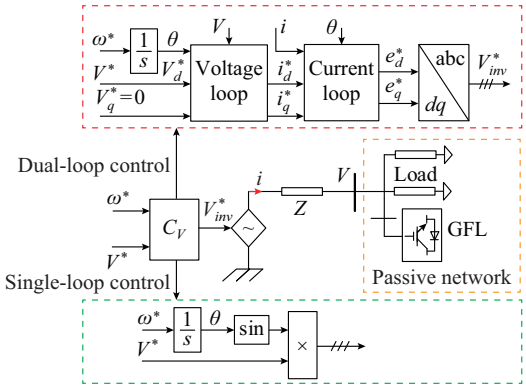

Fig. 6. Structure of VF control.

B. PSL-based GFM control

When integrating with active power grids, the GFM converter is required to have the ability to share power with other voltage sources. Based on the VF control, the PSL is designed to mimic the rotor characteristics of SG, which has the ability of power-sharing, grid-supporting, and self-synchronization with grids. The general structure of the PSL-based GFM control is shown in Fig. 7, where QCL denotes

the reactive power control loop.

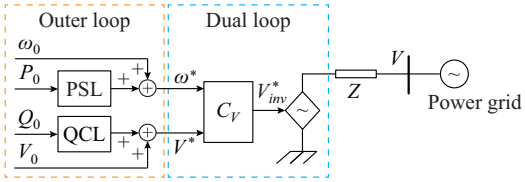

Fig. 7. Basic structure of PSL-based GFM control [15].

According to different structures of PSL, the common PSL-based GFM control includes droop control, power synchronization control (PSC), VSG, synchronverter, synchronous power controller (SPC), etc. Specifically, the structures of these control structures are shown in Fig. 8.

1) Droop Control

In Fig. 8(a), the droop control is designed in accordance with the steady-state droop characteristics of SGs.

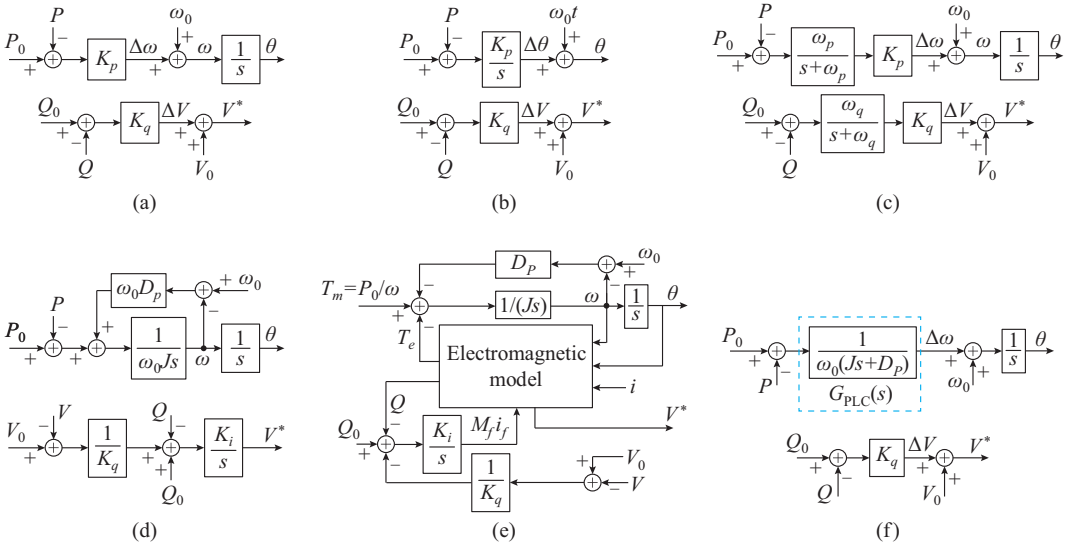

Fig. 8. Different control structures of the PSL-based GFM control. (a) Droop control. (b) PSC. (c) Low-pass filter (LPF) droop control. (d) VSG. (e) Synchronverter. (f) SPC.

In the steady state, the droop characteristics of SGs can be obtained from (2) by letting $\mathrm{d}\omega/\mathrm{d}t=0$. Replacing P_e with the converter power P, the PSL can be designed as:

$$\omega-\omega_0=-\frac{1}{\omega_0 D_P}\left(P-P_0\right)\Leftrightarrow\Delta\omega=-K_p\Delta P \tag{3}$$

where the droop coefficient K_p of PSL is $1/(\omega_0 D_P)$. The design of the QCL refers to the Q-V droop characteristics of SGs, which is:

$$V-V_0=-K_q\left(Q-Q_0\right)\Leftrightarrow\Delta V=-K_q\Delta Q \tag{4}$$

where K_q is the droop coefficient of QCL. With the PSL designed from (3) and (4), the GFM converter can mimic the droop characteristics of SG and share the load power change with other voltage sources (SGs and droop-controlled GFM converter).

Comparing (3) with (2), the inertia term in (3) is missing, which also means that the droop control lacks inertia support capability.

2) PSC

As can be observed from Fig. 8(b), PSC is similar to the droop control. The difference is that the power deviation is used to adjust the frequency in droop control. Due to the lack of inertial emulation, the difference between them will not cause different results [39].

3) LPF Droop Control

In practical projects, to eliminate the sampling ripple in power measurements, the LPFs are commonly added to the droop control, which is shown in Fig. 8(c) [40]. The transfer function of LPF can be expressed as:

$$LPF(s)=\frac{K}{1+\dfrac{s}{\omega_C}} \tag{5}$$

where K is the gain coefficient; and ω_C is the desired cut-off frequency, which is represented by ω_p and ω_q in Fig. 8(c). According to the control structure in Fig. 8(c), the dynamic characteristics of LPF droop control can be obtained as:

$$\frac{1}{\omega_p}\dot{\omega}+\left(\omega-\omega_0\right)=P_0-P \tag{6}$$

It can be found that due to the existence of LPFs, the inertia term exists in (6), which introduces an inertia simulation to the converter dynamic. Thus, the LPF droop control can provide inertia support to suppress the frequency fluctuation of the power grid.

4) VSG Control

Similar to the principle of current-controlled VSG control shown in Fig. 5, the active power control of VSG control also refers to the swing equation (1). Hence, VSG converters can simulate the moment of inertia and the damping characteristics of the rotor. But the difference from current-controlled VSG control is that the VSG control behaves like a controlled voltage source [18]. Besides, the Q-V droop is implemented by adjusting the reactive power reference according to the voltage difference. And the reactive power error is processed by an integrator to obtain V^*, with K_i being the integral gain.

5) Synchronverter

Based on the VSG, the excitation characteristics of SGs have been further considered in the design of synchronverter. Therefore, the synchronverter mimics the operation characteristics of SGs more comprehensively. As shown in Fig. 8(e), according to the electromagnetic model of SG, the electromagnetic torque T_e and the induced electromotive force e can be obtained as [19], [20]:

$$e=\dot{\theta}M_f i_f \tilde{\mathbf{sin}}\,\theta \tag{7}$$

$$P=\dot{\theta}T_e=\dot{\theta}M_f i_f\left\langle i,\tilde{\mathbf{sin}}\,\theta\right\rangle \tag{8}$$

$$Q=-\dot{\theta}M_f i_f\left\langle i,\tilde{\mathbf{cos}}\,\theta\right\rangle \tag{9}$$

$$\begin{cases}\tilde{\mathbf{sin}}\,\theta=\begin{bmatrix}\sin\theta\\ \sin(\theta-2\pi/3)\\ \sin(\theta+2\pi/3)\end{bmatrix}\\ \tilde{\mathbf{cos}}\,\theta=\begin{bmatrix}\cos\theta\\ \cos(\theta-2\pi/3)\\ \cos(\theta+2\pi/3)\end{bmatrix}\end{cases} \tag{10}$$

where $\boldsymbol{i}=[i_a,i_b,i_c]^T$; $\langle\cdot,\cdot\rangle$ denotes the conventional inner product; M_f is the mutual inductance between the rotor coils and the stator coils; and i_f is the excitation current in the rotor.

6) SPC

The structure of the SPC is shown in Fig. 8(f). By designing the power control as a second-order overdamped system, the SPC can overcome the inherent power oscillation issue of SGs under grid disturbances [22], [23]. According to the active power-angle characteristics of voltage sources, it yields:

$$P=P_{\max}\sin\delta\approx P_{\max}\delta \tag{11}$$

where $P_{\max}$ is the maximum output power of the converter; and $\delta=\theta-\theta_{grid}$. Assuming $G_{\mathrm{PLC}}(s)=1/[\omega_0(Js+D_P)]$ is the first-order transfer function, the closed-loop active power control shown in Fig. 9 can be obtained.

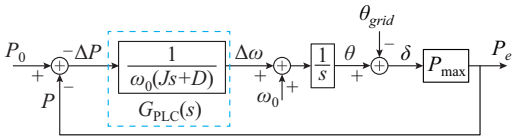

Fig. 9. Closed-loop structure of active power control.

Thus, the closed-loop transfer function of the active power control is second-order and can be expressed as:

$$\frac{P}{P_0}=\frac{\omega_n^2}{s^2+2\xi\omega_n s+\omega_n^2} \tag{12}$$

$$\begin{cases}\xi=\dfrac{D}{2}\sqrt{\dfrac{\omega_0}{JP_{\max}}}\\ \omega_n=\sqrt{\dfrac{P_{\max}}{J\omega_0}}\end{cases} \tag{13}$$

According to (13), the damping coefficient ξ and the undamped natural oscillation angular frequency ω_n of the second-order system can be pre-set by adjusting D and J of $G_{\mathrm{PLC}}(s)$, respectively. Thus, the closed-loop active power control can be further designed as an overdamped system to attenuate the inherent power oscillations of SGs. The $G_{\mathrm{PLC}}(s)$ has many other forms, such as PI controller (additional droop control is required) [21], PI controller integrated with droop control [24], etc. In addition, due to the structure similar to the LPF droop control, the SPC also has the inertia support capability.

According to inertia support capability, the PSL-based GFM control can be further divided into non-inertia control (Fig. 8(a) and (b)) and inertia control (Fig. 8(c)-(f)). Referring to the analysis of the closed-loop active power control of PSC, it can be found that the closed-loop active power control of the inertia control is a second-order system, while that of the non-inertia control is a first-order one.

C. VOC

Unlike PSL-based GFM control, VOC is proposed to make use of the inherent synchronization characteristics of the coupled oscillator network. The VOC converter can generate sinusoidal voltage independently by emulating the dynamic characteristics of the weakly nonlinear oscillator [25]. Compared with the PSL-based GFM control, the VOC does not require multi-loop hierarchical control, nor does it require the voltage amplitude and frequency measurements, which makes VOC much faster in terms of synchronization speed and power-sharing [41], [42]. The commonly used VOC is based on the Van der Pol oscillator, as shown in Fig. 10, where k_v and k_i are the voltage and current gains, respectively; L_v, C_v, and σ are the virtual inductor, capacitor, and resistor of the virtual oscillator circuit, respectively, which is realized through a digital microcontroller; and PWM is the pulse width modulation module.

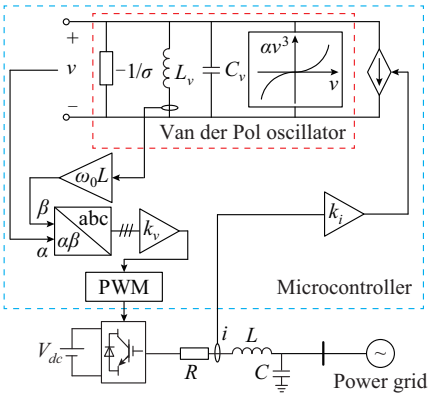

Fig. 10. Structure of VOC based on Van der Pol oscillator.

References [43]-[45] compare VOC and droop control in time domain, and reveal that VOC has steady-state characteristics similar to droop control in the AC cycle scale.

However, the VOC shown in Fig. 10 cannot regulate its output power. To overcome this issue, some additional control loops are added to VOC. In [46] and [47], two PI controllers are adopted to regulate output power by controlling the output current. While in [48], a hierarchical control is introduced to VOC. In addition, different from these methods

adding additional control to VOC, the dispatched VOC (dVOC) is proposed in [49], which is shown in Fig. 11.

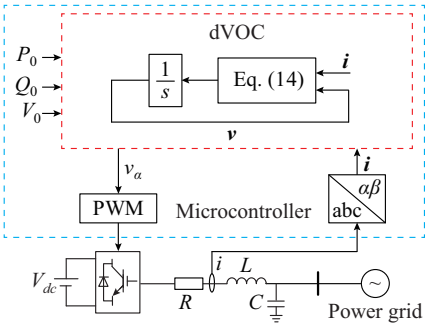

Fig. 11. Structure of dVOC.

In Fig. 11, (14) is defined as:

$$\frac{\mathrm{d}}{\mathrm{d}t}\boldsymbol{v}=\omega_0\boldsymbol{J}\boldsymbol{v}+\eta\left(\boldsymbol{K}\boldsymbol{v}-\boldsymbol{R}(\kappa)\boldsymbol{i}+\alpha\phi(\boldsymbol{v})\boldsymbol{v}\right) \tag{14}$$

where $\boldsymbol{v}=[v_\alpha,v_\beta]^{\mathrm{T}}$, $\boldsymbol{i}=[i_\alpha,i_\beta]^{\mathrm{T}}$; η and α are the positive gain constants; $\boldsymbol{J}=\boldsymbol{R}(\pi/2)$; and $\boldsymbol{R}(\kappa)$, $\boldsymbol{K}$, and the real number $\phi(\boldsymbol{v})$ are expressed as:

$$\begin{cases}\boldsymbol{R}(\kappa)=\begin{bmatrix}\cos\kappa & -\sin\kappa\\ \sin\kappa & \cos\kappa\end{bmatrix}\\ \boldsymbol{K}=\dfrac{1}{V_0^2}\boldsymbol{R}(\kappa)\begin{bmatrix}P_0 & Q_0\\ -Q_0 & P_0\end{bmatrix}\\ \phi(\boldsymbol{v})=\dfrac{V_0^2-\|\boldsymbol{v}\|^2}{V_0^2}\end{cases} \tag{15}$$

where $\|\boldsymbol{v}\|$ is the Euclidean norm of matrix $\boldsymbol{v}$, which means the amplitude of $\boldsymbol{v}$, represented by V; and κ is selected according to the line parameters. For inductive lines, $\kappa=\pi/2$; for resistive lines, $\kappa=0$. Moreover, choosing $\kappa=\pi/2$, the steady-state droop characteristics of dVOC can be expressed as:

$$\begin{cases}\dfrac{\mathrm{d}}{\mathrm{d}t}\theta=\omega=\omega_0+\dfrac{\eta\alpha}{V_0^2}\left(P_0-P\right)\\ V=\|\boldsymbol{v}\|\approx V_0+\dfrac{1}{\alpha V_0}\left(Q_0-Q\right)\end{cases} \tag{16}$$

Reference [50] provides another dVOC on the basis of the Hopf-type oscillator, which is shown in Fig. 12, where v_m and i_m are the virtual controlled voltage source and current source in virtual oscillator circuit, respectively. Its dynamic equation can be obtained as:

$$\begin{cases}\dfrac{\mathrm{d}}{\mathrm{d}t}\theta=\omega=\omega_0-\dfrac{k_v k_i}{3C_v V^2}\left(P-P_0\right)\\ \dfrac{\mathrm{d}}{\mathrm{d}t}V=\dfrac{\xi}{k_v}V\left(2V_0^2-2V^2\right)-\dfrac{k_v k_i}{3C_v V}\left(Q-Q_0\right)\end{cases} \tag{17}$$

According to (16) and (17), ignoring the voltage dynamics, it can be found that the closed-loop active power control of dVOC is also a first-order system, which is a non-inertia control like droop control.

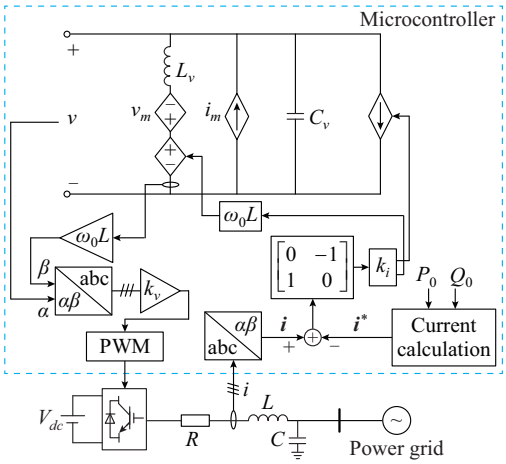

Fig. 12. Hopf-type oscillator based dVOC.

IV. Current Limiting Strategies of GFM Converter

Due to the voltage source characteristic, the GFM converter may encounter overcurrent problems under large grid disturbances, such as AC faults. To ensure the safety of power semiconductors, the current limiting strategies for AC fault are necessary for GFM converter. There are two classic fault current limiting strategies, i. e., the instantaneous saturation limiter and the latched limiter. They are both realized by adding the current limiter block between voltage and current control [51].

The instantaneous saturation limiter of the current reference is expressed as:

$$I'_{ref}=\begin{cases}I_{th} & I_{ref}>I_{th}\\ -I_{th} & I_{ref}<-I_{th}\\ I_{ref} & \text{otherwise}\end{cases} \tag{18}$$

where I_{ref} is the output of the voltage control; I_{th} is the threshold of the current limiter; and I'_{ref} is the limited current reference. Moreover, the instantaneous saturation limiter can be applied in the stationary reference frame (STRF), the synchronous reference frame (SYRF), and the natural reference frame (NARF), which are depicted in Fig. 13 [30], [52]. For the limiters in NARF and STRF, the output of the proportional resonant (PR) controller in voltage control is sinusoidal. When the amplitude of those sine signals ($I_{i,ref}$, $i=a,b,c$ or α,β) exceeds the threshold I_{th}, the sine signal will be clipped and the current reference values $I'_{i,ref}$ have the distortion problem [52]. Thus, the sine signal limiter is proposed to avoid the clipping of sine signals in NARF and STRF, as shown in Fig. 14, where the root meam square (RMS) modular is used to calculate the value of the sine signals [53].

The latched limit strategy means that the current reference I_{ref} will be switched to their pre-defined value I_{sat} once the magnitude exceeds the threshold. Thus, the clipping of the signal can be avoided. The latched limiters in different reference frames are shown in Fig. 15, where I_{sat} is commonly set as a pure reactive current to provide voltage support during AC faults [54]. As can be observed from Fig. 15 [30], [55], the reference switching in each phase is independent in NARF.

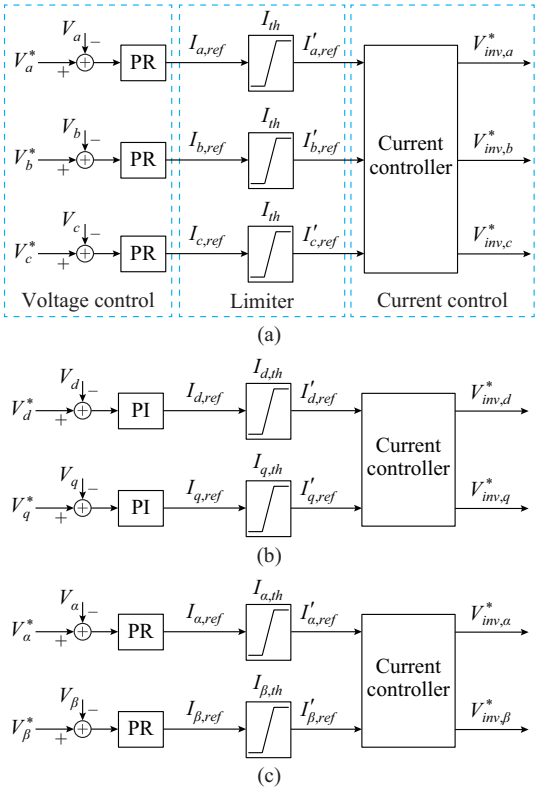

Fig. 13. Instantaneous saturation limiter in different reference frames. (a) NARF. (b) SYRF. (c) STRF.

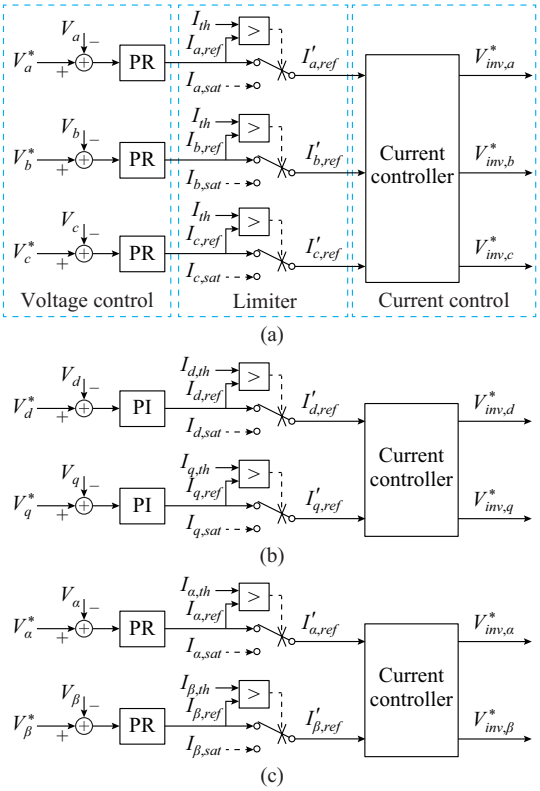

Fig. 15. Latched limiter in different reference frames. (a) NARF. (b) SYRF. (c) STRF.

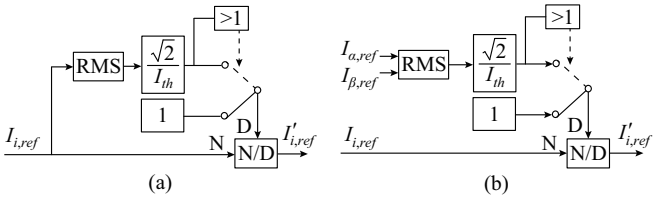

Fig. 14. Sine signal limiter in NARF and STRF. (a) NARF. (b) STRF.

However, for the limiters in SYRF and STRF, all current reference coordinates will be switched to pre-defined values once the magnitude exceeds the threshold, which will cause the same injected current in three phases. As a result, there will be a large converter current injected into healthy phase under asymmetric faults, which may cause overvoltage in healthy phases.

Regarding the overvoltage issue of the limiters in SYRF and STRF, the limiter in NARF shows the merits in controlling each phase current independently. Since the current reference of healthy phases will not be switched to the pre-defined value when the phase fault current exceeds the threshold, the overvoltage issue of healthy phases is avoided. However, this conclusion only applies to three-phase four-leg converters. For the common three-phase three-leg converters in three-wire AC power grids, the sum of three-phase output currents is always zero due to the absence of neutral lines. Thus, there will be no zero-sequence fault current in this system under any faults. However, under asymmetric non-ground faults, the current reference may contain a zero-sequence component due to the separate phase current limit of the NARF limiter.

This zero-sequence current reference may cause the control error of the current controller. Under this circumstance, the outer voltage control of each phase will be saturated. And the current reference I'_{ref} will increase to its maximum limit. The overvoltage issue of healthy phases still exists.

To further overcome the overvoltage issue of the common three-phase three-leg converters, some improvement methods have been proposed. The first method is the parallel virtual impedance method [55], [56]. By utilizing additional virtual impedance control, the output impedance can be greatly reduced. Hence, the overvoltage of healthy phases can be mitigated even under a large current. The second method is the unbalance current injection method [57]. By injecting a small current in healthy phases, the overvoltage can be avoided. But the current reference should meet the current constraint of the three-wire AC power grids. The third method is the hybrid reference frame (HBRF) method [54], [58], [59]. By arranging the controller and limiter in different reference frames, the merits of current limiting strategies in different reference frames can be synthesized. For example, [58] applies the instantaneous saturation limiter in NARF to avoid large current in healthy phases, and utilizes the controller in SYRF to suppress the zero-sequence current, which is shown in Fig. 16.

Most existing studies on current limiting strategies of GFM converters only focus on the performance of current limiting function, and rarely involves the analysis of impact on the transient stability of the converter. In fact, when the fault current exceeds the limiter threshold, the current reference is saturated, which will change the operation mode of GFM converters from voltage source mode to current source mode.

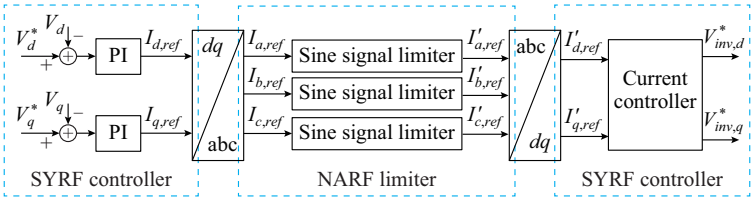

Fig. 16. Current limiting strategies in HBRF [58].

Under this circumstance, a large input error of the PSL during faults may cause a large output frequency deviation. Meanwhile, the power angle of converters will increase continuously, leading to the loss of synchronization. The detailed impact of the current limiting strategies on transient stability will be presented in Section V-B.

V. Stability Analysis of GFM Converters

Stability analysis is another factor to evaluate the performance of GFM control strategies. Thus, the small-signal and transient stability of GFM converters need to be investigated.

A. Small-signal Stability of GFM Converter

The small-signal stability of converters is defined as the ability of the converters to automatically return to the initial operating state without spontaneous oscillation or aperiodic out-of-step when subjected to small disturbances.

In strong active power grids, it is difficult for GFM converters to regulate the point of common coupling (PCC) voltage, which can easily cause oscillation and small-signal instability. According to the oscillation frequency, the instability phenomenon of GFM converters can be divided into sideband oscillations (low-frequency oscillation) and synchronous oscillations (near nominal frequency oscillation) [60]. Based on the state-space small-signal analysis method, [61] reveals the main factors that influence the small-signal stability are voltage feedback decoupling loop and the parameters of the PSL, e. g., the droop coefficient and the operating points.

In weak active power grids with large integration of RESs, it can be proven that GFM converters have robust small-signal stability [17], [62]. The integration of GFM converter also enhances the grid strength due to its voltage regulation capability [37]. Thus, the GFM converters are widely used to overcome the small-signal instability when integrated with weak active power grids [62]-[64].

In particular, for extremely weak active power grids, e.g., 100% GFM converter based network, the control parameters of the power control loop are regarded as the key factors affecting the small-signal stability of the overall system [65] - [71]. Specifically, these key parameters can be determined by the state-space analysis method. For the LPF droop converters, the droop coefficients are key parameters, which affect low-frequency dominant eigenvalues of the system state matrix [38]. Reference [66] points out that the virtual impedance is also the key parameter. For VSG converters, the virtual moment of inertia J and the damping coefficient D are key parameters [67]-[69]. In addition, a similar conclusion is drawn in [70] for synchronverter converter. It also points out that the virtual impedance is the key parameter. The small-signal stability of dVOC converters in Fig. 11 is analyzed in [71], which indicates that the gains η and α are key parameters.

The aforementioned state-space and impedance analysis methods are the commonly-used stability analysis methods. The state-space method is detailed but suffers from high complexity with the increase of system size. Compared with the state-space method, the impedance analysis method only requires the output voltage and current measurements, which has stronger practicability. The impedance analysis method also contains sequence-impedance modeling [72] - [75] and *dq*-impedance modeling [76]-[78]. Except for state-space and impedance analysis methods, the analysis methods for terminal characteristics considering the fundamental frequency dynamics of the grid have been proposed recently, which can reflect the low-frequency stability [79], [80].

B. Transient Stability of GFM Converter

As analyzed in Section IV, when subjected to a large disturbance (i.e., AC fault), the current limiter of GFM converters may saturate and the operation mode of converters will change from the voltage source mode to the current source mode. Therefore, to comprehensively study the transient stability of the GFM converters, both operation modes should be considered.

1) Voltage Source Mode

Under a slight AC grid fault, the converter current will not exceed the threshold and the converters remain in voltage source mode. Thus, the power control loop of GFM converters is still available. According to the analysis in Section III, the active power control loop of non-inertia GFM control is a first-order system. While for inertia control, it is a second-order one. According to the dynamic characteristics of the second-order system, power oscillations may occur if there is no sufficient damping, which will deteriorate the stability of inertia GFM converters [81].

References [30] - [32] analyze the stability of the inertia and non-inertia GFM control by the phase portrait ($\dot{\delta}$ - δ curve) method, as shown in Fig. 17. In the normal operation, the phase portrait is plotted using curve I in Fig. 17. The operating point of the system is stable at the equilibrium point δ_0. Under a slight fault, the PCC voltage sags slightly, and the phase portrait switches to curve II. The operating point will move from δ_0 to a new equilibrium point δ_s or point δ_u. Regarding different GFM control methods, the moving trajectory of the operating point is also different. For non-inertia control, due to the no-overshoot characteristics of the first-order system, the operating point jumps onto curve II, and moves along curve II to the stable equilibrium point δ_s. Thus, non-inertia control converters can maintain stable. But

for the inertia control, its second-order dynamic characteristic will cause the operating point to deviate from curve II. Moreover, a large overshoot will arise under weak damping, which may cause the maximum power angle δ_m to exceed the unstable equilibrium point δ_u. In this case, the inertia control converters may lose their stability even with the existence of the stable equilibrium point δ_s.

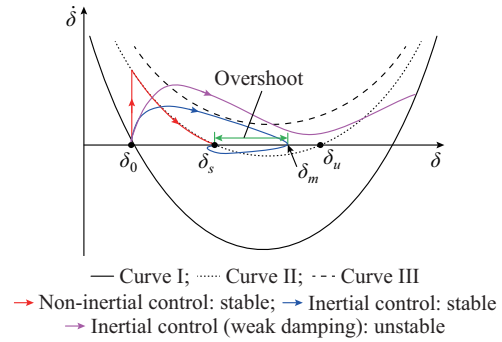

Fig. 17. Phase portrait of inertia and non-inertia GFM control [31].

In conclusion, non-inertia control converters have stronger transient stability than inertia control converters. However, due to the absence of inertia support, the non-inertia GFM converters can endanger the frequency stability of the power system. Therefore, the inertia GFM converters are still required in the power system.

To enhance the transient stability of the inertia GFM converters, [82] and [83] introduce the alternative virtual inertia control to optimize the dynamic performance of converters. Reference [84] presents a method to switch the positive feedback mode of the power-angle control to the negative feedback mode, which can avoid instability even without the equilibrium points.

Notably, the above transient stability analysis is performed in a strong active power grid. For weak active power grids, e. g., RESs dominated grid, the system frequency is mainly dominated by the output frequency of converters. During the transient process, the frequency of the PCC will vary following the output frequency of the connected converter. The difference between PCC frequency and converter frequency may be negligible, and the phase angle difference δ is approximately constant. In this case, the conventional transient stability analysis methods based on the change of δ to evaluate transient stability are no longer applicable, e. g., the phase portrait method in Fig. 17.

To solve this issue, referring to the concept of the center of inertia (COI) in the conventional power system introduced by [85], the COI in converter-dominated power grids is proposed in [86]-[89]. Since the information of COI reflects the global change of the overall system, the transient stability analysis using COI information can be an efficient guidance to improve the consistency and stability of the system [88], [89].

2) Current Source Mode

When a serious AC fault occurs, e.g., a three-phase fault, the current limiter will be saturated and the converter will work in current source mode. To analyze the transient stability in current source mode, [29] and [90] propose a transient stability analysis method based on "virtual power angle" and "virtual power angle curve", which is similar to SGs. Taking the non-inertial GFM control as an example, the virtual power angle curve method is shown in Fig. 18.

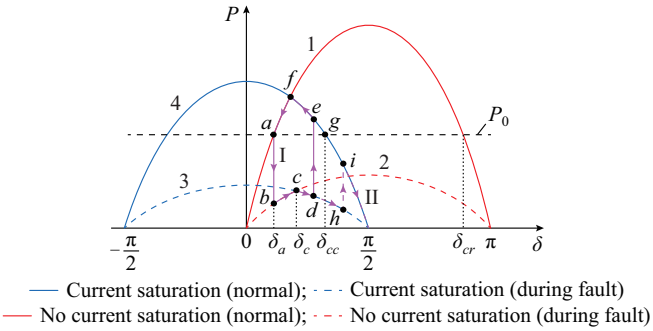

Fig. 18. Virtual power curve of non-inertia control.

Before the saturation of the current limiter, the GFM converter still operates in the voltage source mode. Thus, the power angle curves of the converter during normal operation and faults are similar to those of SGs, which are shown as curves 1 and 2 in Fig. 18, respectively. Once the current limiter saturates, the GFM converter switches to current source mode. The corresponding power angle curve during normal operation and fault conditions can be illustrated as curves 3 and 4 in Fig. 18, respectively [90]. At the initial state, the system operates at point a on curve 1. When a fault occurs, the operating point jumps to point b. Due to the unbalance between P and P_0, the operating point will move to point c along curve 2. At point c, the current limiter saturates, and the converter works in the current source mode. Thus, with the increase of angle, the operating point will continue to move along curve 3. If the fault is cleared before the angle reaches critical clearing angle δ_{cc}, the operating point will move to point e and finally return to point a, as shown in curve I. Otherwise, the operating point will move along curve II, and the angle will lose synchronization. Compared with the normal critical clearing angle in voltage source mode δ_{cr}, δ_{cc} is smaller. Thus, the saturation of current limiter reduces the stability margin of GFM converters.

As analyzed above, the essential reasons for the transient stability issues caused by the current limiter can be concluded as: ① the saturation of current limiter reduces the critical clearing angle δ_{cc}; ② the input error of PSL causes the power angle to increase continuously and exceed the critical clearing angle in the power-angle curve.

To overcome these issues, existing improved current limiting strategies have three main methods: ① the method of switching control mode; ② the method of avoiding operating mode change; ③ the method based on power-angle curve [91]-[94].

1) Method of switching control mode

The method of switching control mode is to switch the GFM control to GFL control mode when the fault is detected, as shown in Fig. 19 [91]. This method is similar to the latched limit strategy. To avoid the input error issue caused by PSL, the PLL is adopted to maintain the synchronization with the power grid. Moreover, this mode switching method

can also be applied in NARF, STRF, and STRF [30]. In addition, this method requires accurate detection of the fault occurrence and clearance to provide switching signals.

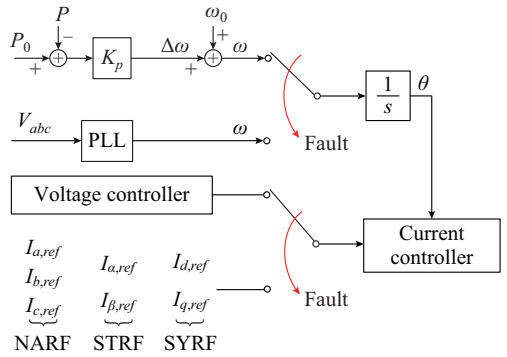

Fig. 19. Mode of switching control method.

2) Method of avoiding operation mode change

To avoid the saturation of current limiters, the virtual impedance based voltage limiting strategy and the power limiting strategy have been proposed to reduce the current reference during AC faults.

The virtual impedance based voltage limiting strategy is designed to add a virtual output impedance to reduce the AC voltage reference V^* when the current exceeds the threshold. Thus, the voltage control loop will not wind up and the current reference will decrease, which can avoid the saturation of current limiters [36]. However, the selection of virtual impedance depends on the fault location and fault types. Thus, the constant virtual impedance is inapplicable to all faults. Aiming at this issue, [53] proposes the adaptive virtual impedance method, which can adaptively regulate the virtual impedance against different faults.

For the power limiting strategy, the current is limited by reducing the power reference during faults [92]. To improve the response speed, the power limiting strategy combined with the instantaneous saturation limiter is proposed in [21]. The instantaneous saturation limiter can limit current quickly, while the power limiting can avoid the saturation of the current limiter. Similarly, the strategy combining power limiting and voltage limiting is proposed in [90].

In summary, the basic idea behind the methods of avoiding operation mode change lies in reducing the references of active quantity (P^*) and reactive quantity (Q^* and V^*) to maintain the outer loop control available and avoid the saturation of the current control loop.

3) Method based on modified power-angle curve

The method based on the modified power-angle curve is to modify the power-angle curve to satisfy the equal-area criterion through additional control. Reference [93] modifies the power-angle curve with improved droop control so that there are still equilibrium points for the power-angle curve even under severe faults. In [94], a method based on adaptive virtual inertia and damping coefficient is proposed to extend the critical clearing angle.

In summary, the grid-tied GFM control can be summarized and compared in terms of control structures, operation characteristics, small-signal stability, and transient stability, etc., as concluded in Table I, where '/' represents no reference mentions, '√' represents the control with this capability; and '×' represents the control without this capability.

VI. Applications of GFM Control

A. Application in AC Microgrids

In AC microgrids, distributed generators (DGs) are commonly connected to power grids via the GFL converters. Under grid disturbances, the frequency fluctuation caused by low-inertia is the major stability issue in microgrids. To improve the stability of the microgrids, GFM control is promising for grid-tied converters [95]. Extensive research has generally applied GFM control in the grid-tied converters of RESs, such as wind power, solar power, and energy storage, which can provide inertia support for microgrids. Except for the application in RESs, some researchers have also emphasized the application at the load side, e.g., electrical vehicles (EVs) [96]. By implementing the GFM control in converters of charging stations, the EVs can behave like an energy storage device to provide grid support similar to RESs [97].

Although the GFM converters have superior performance, there are still some noteworthy problems, e.g., the reactive power sharing error between parallel converters caused by the mismatch of output impedance or line impedance, and the power decoupling error caused by the resistive lines in low-voltage microgrids.

Regarding the power-sharing between parallel converters, the converters require sharing load power change according to their respective capacity to avoid overload [98]. Taking droop control as an example, the principle of reactive power-sharing is illustrated in Fig. 20.

Assuming there are two parallel GFM converters GFM1 and GFM2 with capacities of S_{N1} and S_{N2}, respectively, the output voltage of two converters can be obtained from the Q-V droop control shown in Fig. 20(b), which can be expressed as:

$$\begin{cases} V_{M1} = V_0 - k_1 Q_1 \\ V_{M2} = V_0 - k_2 Q_2 \end{cases} \tag{19}$$

where V_{M1} and V_{M2} are the output voltages of GFM1 and GFM2, respectively; and k_1 and k_2 are the droop coefficients. According to Fig. 20(a), the relationship between V and V_{PCC} is given by (assuming $X >> R$, and ignoring the resistance of line):

$$\begin{cases} V_{M1} = V_{PCC} + \dfrac{X_{L1} Q_1 + R_1 P_1}{V_{PCC}} \\ V_{M2} = V_{PCC} + \dfrac{X_{L2} Q_2 + R_2 P_2}{V_{PCC}} \end{cases} \tag{20}$$

Substituting (20) into (19), we can obtain:

$$\begin{cases} -k_1 Q_1 = V_{PCC} + \dfrac{X_{L1} Q_1}{V_{PCC}} - V_0 \\ -k_2 Q_2 = V_{PCC} + \dfrac{X_{L2} Q_2}{V_{PCC}} - V_0 \end{cases} \tag{21}$$

TABLE I
PERFORMANCE COMPARISON OF DIFFERENT GFM CONTROL METHODS

GFM control		Reference (partial)	Primary frequency/voltage regulation	Inertia support	Power control loop	Transient stability (no current saturation)	Key parameters of small-signal stability	Operation characteristics	Applicable scenarios
VF control		[15]	×	×			/	Constant voltage source	Only passive power grids
PSL-based GFM control	PSC	[17]	√	×	First-order	Strong	/	Imitate droop characteristic of SGs	Active power grids + passive power grids
	Droop	[39]	√	×	First-order	Strong	/		
	LPF droop	[40]	√	√	Second-order	Weak	K_p, K_q (virtual impedance R_V, L_V)	Eliminate the measurement power fluctuation	
	VSG	[67]	√	√	Second-order	Weak	J, D_p (R_V, L_V)	Imitate SGs characteristics in detail	
	Synchronverter	[18], [70]	√	√	Second-order	Weak	J, D_p	Based on VSG, consider excitation characteristics	
	SPC	G_{PLC}:= $1/[\omega_0(Js+D_p)]$ [22], [23]	√	√	Second-order	Weak	ξ (J, D_p)	Design an overdamped response to suppress power fluctuation	
		GPLC is PI controller [21]	√	√	Second-order	Weak	ξ (PI controller parameters K_P, K_I)	Need extra droop control	
		G_{PLC} is droop PI controller [24]	√	√	Second-order	Weak	ξ (Improved PI controller parameters K_P, K_I, K_G)	Need no extra droop control	
VOC-based GFM control		VOC (Van der Pol) [25], [41]	√	×	First-order	Strong	/	Synchronize from any initial condition, need no measurement and calculation of voltage and power	Active power grids + passive power grids
		dVOC [49]	√	×	First-order	Strong	η, α		
		dVOC (Hopf-type) [50]	√	×	First-order	Strong	/	Directly control power without extra control loop	

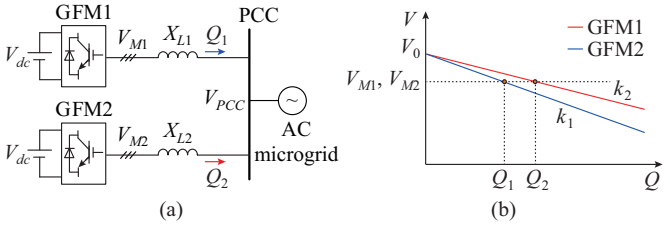

Fig. 20. Illustration of reactive power-sharing. (a) Topology of parallel converters. (b) Q-V droop control of converters.

To share the reactive power according to the converter capacity, the droop coefficients are commonly set as:

$$k_1/k_2 = Q_2/Q_1 = S_{N2}/S_{N1} \tag{22}$$

Referring to (21), the line impedances X_{L1} and X_{L2} should satisfy:

$$X_{L2}/X_{L1} = S_{N1}/S_{N2} = k_2/k_1 \tag{23}$$

In fact, owing to different distances from converters to PCC, the line impedance may not meet (23), which will cause reactive power sharing error ($k_1Q_1 \neq k_2Q_2$). The large power error may result in a large circulating current between converters and even damage the converters. While for active power sharing, since the frequency cannot be affected by the line impedance, active power can be shared according to the converter capacity without error [99], [100].

To eliminate the reactive power sharing error, the virtual impedance control is regarded as a promising solution [101]-[103]. By introducing large matched virtual impedances in parallel converters, the mismatched line impedance issues can be overcome. The virtual impedance control is shown in Fig. 21, where Z_V is the matched virtual impedance; C_P and C_Q are active and reactive power control loops, respectively.

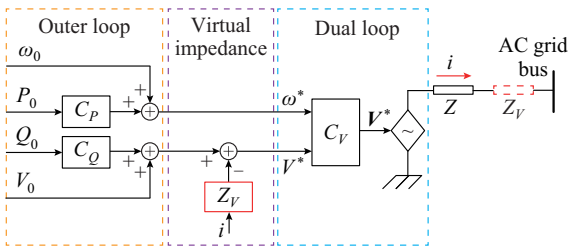

Fig. 21. Illustration of virtual impedance control.

For the power decoupling error, it arouses from the resistive lines, especially in the low-voltage microgrids. Accord-

ing to equation (20), the decoupling design of *P-f* and *Q-V* droop control in GFM converters is commonly based on pure inductive lines. Thus, the resistive lines will increase the coupling between active and reactive power, which will deteriorate the power control accuracy [15], [104].

To overcome the power decoupling error, the virtual impedance control technology is still effective. By introducing a large virtual inductance, the effect of resistive lines can be ignored [105]-[107]. However, the virtual inductance should be selected appropriately. A large virtual inductance will cause a large output voltage sag, which requires compensation [106]. Reference [107] points out that the optimal value of virtual inductance can be obtained by considering the limit of the reactive power capacity of converters. Except for the virtual inductance, the technologies based on virtual complex impedance and virtual negative resistance are also effective [108]-[110].

B. Application in Offshore Wind Farm (OWF) HVDC Systems

The topology of a typical point-to-point HVDC system integrating OWFs is shown in Fig. 22.

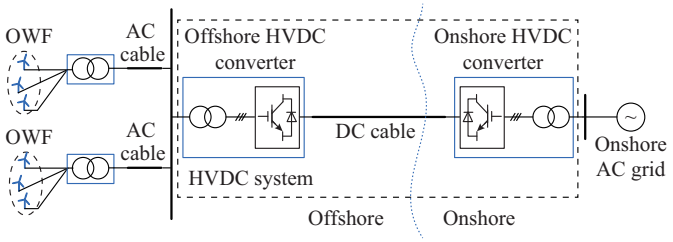

Fig. 22. Topology of OWF-HVDC system.

Due to different technical requirements of various application scenarios, the adopted GFM controls in OWF-HVDC systems are different from those in AC microgrids. Thus, there are some variants of GFM control in OWF-HVDC systems.

1) GFM Control of Offshore HVDC Converter

Since the grid-side converter (GSC) of wind turbine (WT) adopts GFL control, the offshore AC grid is equivalent to a passive grid [111]. Thus, the VF control is commonly applied in offshore HVDC converters to provide a stable AC voltage. In addition to VF control, the PSC with frequency control is also an alternative [112].

2) GFM Control of Onshore HVDC Converter

With the increasing integration of RESs via HVDC systems, the onshore AC grid has potential instability problems, such as low inertia and low short-circuit ratio (SCR). To overcome these issues, the GFM control can be applied in onshore HVDC converters [62]. For typical GFM control introduced in Section III, their self-synchronization strategies are based on active power. However, due to the requirement of DC voltage control, the self-synchronization strategies of the onshore converter are commonly based on DC capacitor voltage (i. e., matching control) [113] - [116]. The matching control methods utilize the physical DC-link capacitor as energy storage, which is like the rotor energy storage of SGs. The similarity between the DC capacitor and the rotor can be revealed by (24) and Fig. 23 [115].

$$\begin{cases} C_{dc}V_{dc}\dfrac{\mathrm{d}V_{dc}}{\mathrm{d}t}=P_{dc}-P_{ac}-TV_{dc} \\ J\omega_m\dfrac{\mathrm{d}\omega_m}{\mathrm{d}t}=P_m-P_e-D_P\omega_m \end{cases} \tag{24}$$

where C_{dc} is the equivalent capacitor of the DC system; and T is the damping coefficient in the DC system.

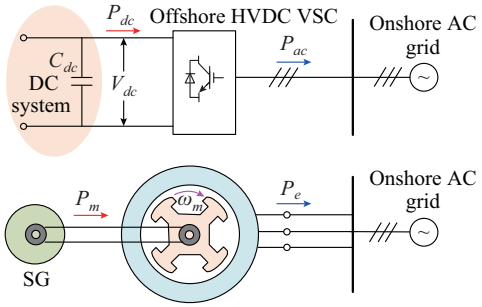

Fig. 23. Principle of matching control.

It can be observed that the DC voltage V_{dc} can reflect the unbalance of power, which is like frequency ω_m. Thus, by coupling V_{dc} with ω_m, the block diagram of self-synchronization control based on the DC capacitor is shown in Fig. 24.

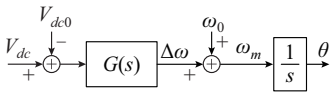

Fig. 24. Matching control coupling V_{dc} and ω_m.

The transfer function $G(s)$ in Fig. 24 is commonly constant when neglecting the dynamic of the V_{dc} and ω_m [114], [117]. However, to achieve that the dynamic of V_{dc} is the same as that of ω_m, the desired $G(s)$ should be obtained from (24), which is rewritten in (25) [115]. In this way, the onshore HVDC converter can accurately mimic the SG characteristics.

$$\begin{aligned} &\omega_m\left(Js+D_p\right)=V_{dc}\left(C_{dc}s+T\right)\Rightarrow\omega_m=\frac{C_{dc}s+T}{Js+D_p}V_{dc}\Rightarrow \\ &G(s)=\frac{C_{dc}s+T}{Js+D_p} \end{aligned} \tag{25}$$

By coupling V_{dc}^2 and ω_m, [113] proposes the self-synchronization strategy shown in Fig. 25.

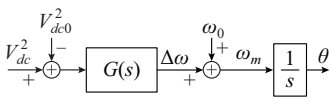

Fig. 25. Matching control coupling V_{dc}^2 and ω_m.

In Fig. 25, $G(s)$ is designed according to (25).

$$G(s)=\frac{s+K_T}{K_Js+K_D} \tag{26}$$

where K_J is the virtual inertia constant; K_D is the damping coefficient; and K_T is the tracking coefficient of the DC link voltage. The relationship between power deviation ΔP and frequency deviation $\Delta\omega$ is illustrated in Fig. 26 [113]. As shown in Fig. 26, this method is consistent with SPC, which

can overcome the inherent power oscillation of SGs.

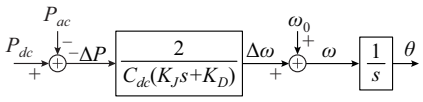

Fig. 26. Block diagram of power-angle control.

3) GFM Control of WT GSC

As mentioned above, the WT GSC commonly adopts the GFL control. However, the offshore AC grid may lose its AC voltage sources in some scenarios. Firstly, the offshore HVDC converter may be blocked or tripped under some accidents, e. g., DC cable faults [118]. Secondly, the offshore HVDC converter is incapable of controlling the voltage and frequency of the offshore grid, such as in the diode rectifier unit (DRU) based HVDC system. To avoid the shutdown of wind farms, the WT GSC is required to adopt GFM control to maintain the offshore grid stable.

In the first scenario, once the offshore converter is blocked, the large power deviation in the offshore grid will cause the saturation of the current integral loop in GSC. And the overvoltage and over-frequency phenomena will occur [118]. To control the grid voltage and frequency, the direct voltage control is proposed by abandoning the current integral loop [118]-[120]. In addition, [121] provides the method of switching control mode. By using the overvoltage characteristics of the offshore grid, the GSC can seamlessly transit from GFL control mode to VF control (GFM) mode.

In the second scenario, since the DRU cannot control the offshore grid, the WT GSC should have the ability to form AC voltage independently [122]. In [123], the strong coupling of *V-P* and *f-Q* in DRU-HVDC are utilized to design the voltage and frequency control, respectively. Whereas, this control requires the communication of the offshore grid voltage from the offshore PCC bus to the WT side. Based on this control principle, [124] further proposes the distributed PLL control based on local measurements without communication. To overcome the power-sharing issue in distributed control, the *P-V* control and *Q-f* droop control are also designed.

VII. Challenges of GFM control

A. Energy Storage of GFM Converter

In previous research works, the GFM control is simply implemented by an ideal DC voltage source connected to the DC side of converters. Actually, energy storage systems (ESSs) should be involved in GFM converters to self-synchronize with grids and provide grid support. Thus, the implementation and coordination control of ESSs in GFM converter are the technical focuses in future applications.

Currently, ESSs can be realized through different approaches, such as flywheel ESSs, superconducting magnetic energy storage, battery energy storage (BES), and energy capacitor storage. So far, the promising ESS topology is the hybrid energy storage system (HESS) [125]. It consists of ultra-capacitors (UC) and BES, which can respond to the grid transient at different varying speeds [126], [127]. The UC is a high-power density storage unit, which is suitable for fast response. The battery is a high-energy-density storage unit, which is suitable for a large energy reserve. In this HESS, the UC can be controlled to generate the power in response to the high rate of change of frequency (RoCoF), and the BES can be used to generate the power in response to low RoCoF. Compared with a single ESS, the HESS has a multi-time-scale response capability. Whereas, HESS needs complex management and control strategies, especially during the charging and discharging of each storage unit. Moreover, there is no guideline on how to design the threshold of RoCoF to trigger different storage units, and it is typically determined through trial and error.

In summary, the selection of energy storage units in an ESS is the first challenge during the design of ESSs, which requires a trade-off among performance, complexity, costs, etc. Then, the coordination of GFM control and ESSs is the other challenge, such as the lack of guidance for parameter design.

B. AC Fault Protection in GFM Converters Interfaced Grid

In a conventional SG-dominated power system, the main AC line protection strategies are designed according to the fault characteristics of SGs, such as overcurrent-based protection, distance protection, zero-/negative-sequence protections and so on. With the large-scale integration of GFM converters, the fault characteristics will be depended on the converter control, which is quite different from SGs. Thus, conventional protection methods may lose their reliability. For example, the unique current limiting control may cause the malfunction of overcurrent protection schemes during AC faults [128]. Moreover, the dual-sequence control of GFM converters also affects the correctness of the negative-sequence protections, such as the negative-sequence component suppression control [129]. In addition, the measured impedance by distance relays is also adversely affected by the fault ride-through control of converters, which reduces the reliability of distance protection [130]. Thus, conventional AC line protections are no longer suitable for power systems integrated with GFM converters. Recently, some scholars propose solutions by modifying the converter control and the protection relay. Reference [131] proposes a soft current limiting control to generate the inter-harmonic current, which can be detected by a designed inter-harmonic differential relay to identify the AC line faults. In [132], through modifying control to inject synthetic harmonic current during AC faults, the relay can measure the harmonic current to identify the fault location.

In conclusion, with the increasing proportion of renewable energy, conventional AC line protections are not reliable. It is necessary to construct new AC protection schemes considering the cooperation of converter control and relay protection elements.

VIII. Conclusion

In RESs dominated power systems, common GFL control shows poor stability and dynamic performance due to its current source characteristics. As a promising alternative, the

GFM control has grid-friendly features, which can work as a voltage source to provide grid support. Considering the control structures, the state-of-the-art GFM control can be divided into VF control, PSL-based GFM control, and VOC-based GFM control.

1) Comparing the small-signal stability of GFM control in different application scenarios, it shows poorer small-signal stability in strong active grids than those in weak active grids. Especially for the GFM converter-based network, the control parameters of the power control loop are the key ones affecting the small-signal stability of the overall system.

2) Considering the saturation of the current limiter, the transient stability of GFM converters in voltage source mode and current source mode are both analyzed. For the converter in voltage source mode, the inertia control shows weaker stability than non-inertia control due to the overshoot of the second-order system. For the converter in current source mode, the saturation of the current limiter reduces the stability margin.

3) By analyzing the applications of GFM control, this paper points out the reactive power sharing error and power decoupling error in AC microgrids. Comparing the variants of GFM control applied in OWF-HVDC systems (includes GSC of WTs, offshore and onshore HVDC converters), these GFM control strategies also show their advantages in VF control, autonomous operation, and strong stability.

4) Nowadays, ESSs with high energy and power densities and accurate coordination control strategies are urgently required for GFM converters. Moreover, due to different fault characteristics of GFM converters, conventional AC line protection methods may be unavailable. These two issues should be handled for the wide applications of GFM converters in the future.

REFERENCES

[1] G. Denis, T. Prevost, M. Debry *et al*., "The Migrate project: the challenges of operating a transmission grid with only inverter-based generation: a grid-forming control improvement with transient current-limiting control," *IET Renewable Power Generation*, vol. 12, no. 5, pp. 523-529, Mar. 2018.

[2] B. Kroposki, B. Johnson, Y. Zhang *et al*., "Achieving a 100% renewable grid: operating electric power systems with extremely high levels of variable renewable energy," *IEEE Power and Energy Magazine*, vol. 15, no. 2, pp. 61-73, Mar. 2017.

[3] Energy Research Institute of the National Development and Reform Commission of the People's Republic of China. (2015, Apr.). 2050 high-proportion renewable energy development scenarios and approaches. [Online]. Available: https://www. efchina. org/Reports-zh/china-2050-high-renewable-energy-penetration-scenario-and-roadmap-study-zh

[4] Y. Liu, S. You, J. Tan *et al*., "Frequency response assessment and enhancement of the U.S. power grids toward extra-high photovoltaic generation penetrations-an industry perspective," *IEEE Transactions on Power Systems*, vol. 33, no. 3, pp. 3438-3449, May 2018.

[5] B. Ni, W. Xiang, M. Zhou *et al.*, "An adaptive fault current limiting control for MMC and its application in DC grid," *IEEE Transactions on Power Delivery*, vol. 36, no. 2, pp. 920-931, Apr. 2021.

[6] T. Ackermann, T. Prevost, V. Vittal *et al*., "Paving the way: a future without inertia is closer than you think," *IEEE Power and Energy Magazine*, vol. 15, no. 6, pp. 61-69, Nov. 2017.

[7] National Grid ESO. (2019, Jan.). Technical report on the events of 9 August 2019. [Online]. Available: https://www.nationalgrideso.com/ information-about-great-britains-energy-system-and-electricity-system-operator-eso

[8] EirGrid SONI. (2012, Mar.). DS3: system services review tso recommendations. [Online]. Available: https://www. eirgridgroup. com/site-files/library/EirGrid/System-Services-TSO-Recommendations-May2013. pdf

[9] Australian Energy Market Operator. (2017, Mar.). Black system South Australia 28 September 2016: final report. [Online]. Available: https:// apo.org.au/node/74886.

[10] L. Fan, *Control and Dynamics in Power Systems and Microgrids*. Boca Raton: CRC Press, 2017.

[11] L. Tom, "Participation of inverter-connected distributed energy resources in grid voltage control," Ph.D. dissertation, Katholieke Universiteit, Leuven, Holland, 2011.

[12] C. Zou, H. Rao, S. Xu *et al*., "Analysis of resonance between a VSC-HVDC converter and the AC grid," *IEEE Transactions on Power Electronics*, vol. 33, no. 12, pp. 10157-10168, Dec. 2018.

[13] H. Liu, X. Xie, J. He *et al*., "Subsynchronous interaction between direct-drive PMSG based wind farms and weak AC networks," *IEEE Transactions on Power Systems*, vol. 32, no. 6, pp. 4708-4720, Nov. 2017.

[14] R. H. Lasseter, Z. Chen, and D. Pattabiraman, "Grid-forming inverters: a critical asset for the power grid," *IEEE Journal of Emerging and Selected Topics in Power Electronics*, vol. 8, no. 2, pp. 925-935, Jun. 2020.

[15] J. Rocabert, A. Luna, F. Blaabjerg *et al*., "Control of power converters in AC microgrids," *IEEE Transactions on Power Electronics*, vol. 27, no. 11, pp. 4734-4749, Nov. 2012.

[16] D. Pattabiraman, R. H. Lasseter, and T. M. Jahns, "Comparison of grid following and grid forming control for a high inverter penetration power system," in *Proceedings of 2018 IEEE PES General Meeting (PESGM)*, Portland, USA, Aug. 2018, pp. 1-5.

[17] L. Zhang, L. Harnefors, and H. Nee, "Power-synchronization control of grid-connected voltage-source converters," *IEEE Transactions on Power Systems*, vol. 25, no. 2, pp. 809-820, May 2010.

[18] N. Soni, S. Doolla, and M. C. Chandorkar, "Improvement of transient response in microgrids using virtual inertia," *IEEE Transactions on Power Delivery*, vol. 28, no. 3, pp. 1830-1838, Jul. 2013.

[19] Q. Zhong, "Virtual synchronous machines: a unified interface for grid integration," *IEEE Power Electronics Magazine*, vol. 3, no. 4, pp. 18-27, Dec. 2016.

[20] Q. Zhong, P. Nguyen, Z. Ma *et al*., "Self-synchronized synchronverters: inverters without a dedicated synchronization unit," *IEEE Transactions on Power Electronics*, vol. 29, no. 2, pp. 617-630, Feb. 2014.

[21] M. G. Taul, X. Wang, P. Davari *et al*., "Current limiting control with enhanced dynamics of grid-forming converters during fault conditions," *IEEE Journal of Emerging and Selected Topics in Power Electronics*, vol. 8, no. 2, pp. 1062-1073, Jun. 2020.

[22] W. Zhang, A. M. Cantarellas, J. Rocabert *et al*., "Synchronous power controller with flexible droop characteristics for renewable power generation systems," *IEEE Transactions on Sustainable Energy*, vol. 7, no. 4, pp. 1572-1582, Oct. 2016.

[23] P. Rodriguez, I. Candela, and A. Luna, "Control of PV generation systems using the synchronous power controller," in *Proceedings of 2013 IEEE Energy Conversion Congress and Exposition*, Denver, USA, Sept. 2013, pp. 993-998.

[24] W. Zhang, D. Remon, and P. Rodriguez, "Frequency support characteristics of grid-interactive power converters based on the synchronous power controller," *IET Renewable Power Generation*, vol. 11, no. 4, pp. 470-479, May, 2017.

[25] B. B. Johnson, S. V. Dhople, A. O. Hamadeh *et al*., "Synchronization of parallel single-phase inverters with virtual oscillator control," *IEEE Transactions on Power Electronics*, vol. 29, no. 11, pp. 6124-6138, Nov. 2014.

[26] M. Ali, H. I. Nurdin, and J. E. Fletcher, "Dispatchable virtual oscillator control for single-phase islanded inverters: analysis and experiments," *IEEE Transactions on Industrial Electronics*, vol. 68, no. 6, pp. 4812-4826, Jun. 2021.

[27] N. Pogaku, M. Prodanovic, and T. C. Green, "Modeling, analysis and testing of autonomous operation of an inverter-based microgrid," *IEEE Transactions on Power Electronics*, vol. 22, no. 2, pp. 613-625, Mar. 2007.

[28] D. Sun, H. Liu, S. Gao *et al*., "Comparison of Different Virtual Inertia Control Methods for Inverter-based Generators," *Journal of Modern Power Systems and Clean Energy*, vol. 8, no. 4, pp. 768-777, Jul. 2020.

[29] H. Xin, L. Huang, L. Zhang *et al*., "Synchronous instability mechanism of *P-f* droop-controlled voltage source converter caused by current saturation," *IEEE Transactions on Power Systems*, vol. 31, no. 6, pp. 5206-5207, Nov. 2016.

[30] H. Wu and X. Wang, "Design-oriented transient stability analysis of grid-connected converters with power synchronization control," *IEEE Transactions on Industrial Electronics*, vol. 66, no. 8, pp. 6473-6482, Aug. 2019.
[31] D. Pan, X. Wang, F. Liu *et al*., "Transient stability of voltage-source converters with grid-forming control: a design-oriented study," *IEEE Journal of Emerging and Selected Topics in Power Electronics*, vol. 8, no. 2, pp. 1019-1033, Jun. 2020.
[32] H. Yu, M. A. Awal, H. Tu *et al*., "Comparative transient stability assessment of droop and dispatchable virtual oscillator controlled grid-connected inverters," *IEEE Transactions on Power Electronics*, vol. 36, no. 2, pp. 2119-2130, Feb. 2021.
[33] J. Z. Zhou, H. Ding, S. Fan *et al*., "Impact of short-circuit ratio and phase-locked-loop parameters on the small-signal behavior of a vsc-HVDC converter," *IEEE Transactions on Power Delivery*, vol. 29, no. 5, pp. 2287-2296, Oct. 2014.
[34] B. Wen, D. Boroyevich, R. Burgos *et al*., "Analysis of *d-q* small-signal impedance of grid-tied inverters," *IEEE Transactions on Power Electronics*, vol. 31, no. 1, pp. 675-687, Jan. 2016.
[35] D. Zhu, S. Zhou, X. Zou *et al*., "Improved design of PLL controller for LCL-type grid-connected converter in weak grid," *IEEE Transactions on Power Electronics*, vol. 35, no. 5, pp. 4715-4727, May 2020.
[36] A. D. Paquette and D. M. Divan, "Virtual impedance current limiting for inverters in microgrids with synchronous generators," *IEEE Transactions on Industry Applications*, vol. 51, no. 2, pp. 1630-1638, Mar.-Apr. 2015.
[37] C. Yang, L. Huang, H. Xin *et al*., "Placing grid-forming converters to enhance small signal stability of PLL-integrated power systems," *IEEE Transactions on Power Systems*, vol. 36, no. 4, pp. 3563-3573, Jul. 2021.
[38] W. Du, Z. Chen, K. P. Schneider *et al*., "A comparative study of two widely used grid-forming droop controls on microgrid small-signal stability," *IEEE Journal of Emerging and Selected Topics in Power Electronics*, vol. 8, no. 2, pp. 963-975, Jun. 2020.
[39] S. D'Arco and J. A. Suul, "Virtual synchronous machines – classification of implementations and analysis of equivalence to droop controllers for microgrids," in *Proceedings of 2013 IEEE Grenoble Conference*, Grenoble, Fance, Jun. 2013, pp. 1-7.
[40] P. Hart and B. Lesieutre, "Energy function for a grid-tied, droop-controlled inverter," in *Proceedings of 2014 North American Power Symposium (NAPS)*, Pullman, USA, Sept. 2014, pp. 1-6.
[41] B. B. Johnson, M. Sinha, N. G. Ainsworth *et al*., "Synthesizing virtual oscillators to control islanded inverters," *IEEE Transactions on Power Electronics*, vol. 31, no. 8, pp. 6002-6015, Aug. 2016.
[42] M. Sinha, F. Dörfler, B. B. Johnson *et al*., "Uncovering droop control laws embedded within the nonlinear dynamics of van der pol oscillators," *IEEE Transactions on Control of Network Systems*, vol. 4, no. 2, pp. 347-358, Jun. 2017.
[43] C. A. Plet, M. Brucoli, J. D. F. McDonald *et al*., "Fault models of inverter-interfaced distributed generators: experimental verification and application to fault analysis," in *Proceedings of 2011 IEEE Power and Energy Society General Meeting (PESGM)*, Detroit, USA, Jul. 2011, pp. 1-8.
[44] D. Sun, H. Liu, S. Gao *et al*., "Comparison of different virtual inertia control methods for inverter-based generators," *Journal of Modern Power Systems and Clean Energy*, vol. 8, no. 4, pp. 768-777, Jul. 2020.
[45] Z. Shi, J. Li, H. I. Nurdin *et al*., "Comparison of virtual oscillator and droop controlled islanded three-phase microgrids," *IEEE Transactions on Energy Conversion*, vol. 34, no. 4, pp. 1769-1780, Dec. 2019.
[46] P. Hazra, R. Hadidi, and E. Makram, "Dynamic study of virtual oscillator controlled inverter based distributed energy source," in *Proceedings of 2015 North American Power Symposium (NAPS)*, Charlotte, NC, USA, Oct. 2015, pp. 1-6.
[47] D. Raisz, T. T. Thai, and A. Monti, "Power control of virtual oscillator controlled inverters in grid-connected mode," *IEEE Transactions on Power Electronics*, vol. 34, no. 6, pp. 5916-5926, Jun. 2019.
[48] M. A. Awal, H. Yu, H. Tu *et al*., "Hierarchical control for virtual oscillator based grid-connected and islanded microgrids," *IEEE Transactions on Power Electronics*, vol. 35, no. 1, pp. 988-1001, Jan. 2020.
[49] G. Seo, M. Colombino, I. Subotic *et al*., "Dispatchable virtual oscillator control for decentralized inverter-dominated power systems: analysis and experiments," in *Proceedings of 2019 IEEE Applied Power Electronics Conference and Exposition (APEC)*, Anaheim, CA, USA, Mar. 2019, pp. 561-566.
[50] M. Lu, S. Dutta, V. Purba *et al*., "A grid-compatible virtual oscillator controller: analysis and design," in *Proceedings of 2019 IEEE Energy Conversion Congress and Exposition (ECCE)*, Baltimore, MD, USA, Oct. 2019, pp. 2643-2649.
[51] N. Bottrell and T. C. Green, "Comparison of current-limiting strategies during fault ride-through of inverters to prevent latch-up and wind-up," *IEEE Transactions on Power Electronics*, vol. 29, no. 7, pp. 3786-3797, Jul. 2014.
[52] M. S. Golsorkhi and D. D. Lu, "A decentralized control method for islanded microgrids under unbalanced conditions," *IEEE Transactions on Power Delivery*, vol. 31, no. 3, pp. 1112-1121, Jun. 2016.
[53] S. F. Zarei, H. Mokhtari, M. A. Ghasemi *et al*., "Reinforcing fault ride through capability of grid forming voltage source converters using an enhanced voltage control scheme," *IEEE Transactions on Power Delivery*, vol. 34, no. 5, pp. 1827-1842, Oct. 2019.
[54] C. A. Plet, "Fault response of inverter-based distributed generation," Ph.D. Dissertation, Imperial College, London, UK, 2012.
[55] C. A. Plet and T. C. Green, "A method of voltage limiting and distortion avoidance for islanded inverter-fed networks under fault," in *Proceedings of 2011 14th European Conference on Power Electronics and Applications*, Birmingham, Sept. 2011, pp. 1-8.
[56] X. Lin, Z. Liang, Y. Zheng *et al*., "A current limiting strategy with parallel virtual impedance for three-phase three-leg inverter under asymmetrical short-circuit fault to improve the controllable capability of fault currents," *IEEE Transactions on Power Electronics*, vol. 34, no. 8, pp. 8138-8149, Aug. 2019.
[57] Z. Liang, X. Lin, Y. Kang *et al*., "Short circuit current characteristics analysis and improved current limiting strategy for three-phase three-leg inverter under asymmetric short circuit fault," *IEEE Transactions on Power Electronics*, vol. 33, no. 8, pp. 7214-7228, Aug. 2018.
[58] I. Sadeghkhani, M. E. H. Golshan, J. M. Guerrero *et al*., "A current limiting strategy to improve fault ride-through of inverter interfaced autonomous microgrids," *IEEE Transactions on Smart Grid*, vol. 8, no. 5, pp. 2138-2148, Sept. 2017.
[59] B. Mahamedi, M. Eskandari, J. E. Fletcher *et al*., "Sequence-based control strategy with current limiting for the fault ride-through of inverter-interfaced distributed generators," *IEEE Transactions on Sustainable Energy*, vol. 11, no. 1, pp. 165-174, Jan. 2020.
[60] X. Wang and F. Blaabjerg, "Harmonic stability in power electronic-based power systems: concept, modeling, and analysis," *IEEE Transactions on Smart Grid*, vol. 10, no. 3, pp. 2858-2870, May 2019.
[61] X. Wang, M. G. Taul, H. Wu *et al*., "Grid-synchronization stability of converter-based resources—an overview," *IEEE Open Journal of Industry Applications*, vol. 1, pp. 115-134, Aug. 2020.
[62] L. Huang, H. Xin, H. Yang *et al*., "Interconnecting very weak ac systems by multiterminal VSC-HVDC links with a unified virtual synchronous control," *IEEE Journal of Emerging and Selected Topics in Power Electronics*, vol. 6, no. 3, pp. 1041-1053, Sept. 2018.
[63] C. Guo, W. Liu, C. Zhao *et al*., "A frequency-based synchronization approach for the VSC-HVDC station connected to a weak AC grid," *IEEE Transactions on Power Delivery*, vol. 32, no. 3, pp. 1460-1470, Jun. 2017.
[64] S. Sang, N. Gao, X. Cai *et al*., "A novel power-voltage control strategy for the grid-tied inverter to raise the rated power injection level in a weak grid," *IEEE Journal of Emerging and Selected Topics in Power Electronics*, vol. 6, no. 1, pp. 219-232, Mar. 2018.
[65] K. Yu, Q. Ai, S. Wang *et al*., "Analysis and optimization of droop controller for microgrid system based on small-signal dynamic model," *IEEE Transactions on Smart Grid*, vol. 7, no. 2, pp. 695-705, Mar. 2016.
[66] H. Xu, C. Yu, C. Liu *et al*., "An improved virtual capacitor algorithm for reactive power sharing in multi-paralleled distributed generators," *IEEE Transactions on Power Electronics*, vol. 34, no. 11, pp. 10786-10795, Nov. 2019.
[67] J. Chen and T. O'Donnell, "Parameter constraints for virtual synchronous generator considering stability," *IEEE Transactions on Power Systems*, vol. 34, no. 3, pp. 2479-2481, May 2019.
[68] W. Du, Q. Fu, and H. F. Wang, "Power system small-signal angular stability affected by virtual synchronous generators," *IEEE Transactions on Power Systems*, vol. 34, no. 4, pp. 3209-3219, Jul. 2019.
[69] B. K. Unnikrishnan, M. S. Johnson, and E. P. Cheriyan, "Small signal stability improvement of a microgrid by the optimised dynamic droop control method," *IET Renewable Power Generation*, vol. 14, no. 5, pp. 822-833, Apr. 2020.
[70] A. Rodríguez-Cabero, J. Roldán-Pérez, and M. Prodanovic, "Virtual impedance design considerations for virtual synchronous machines in weak grids," *IEEE Journal of Emerging and Selected Topics in Power Electronics*, vol. 8, no. 2, pp. 1477-1489, Jun. 2020.
[71] D. Groß, M. Colombino, J. Brouillon *et al*., "The effect of transmis-

sion-line dynamics on grid-forming dispatchable virtual oscillator control," *IEEE Transactions on Control of Network Systems*, vol. 6, no. 3, pp. 1148-1160, Sept. 2019.
[72] M. Cespedes and J. Sun, "Impedance modeling and analysis of grid-connected voltage-source converters," *IEEE Transactions on Power Electronics*, vol. 29, no. 3, pp. 1254-1261, Mar. 2014.
[73] B. Wen, D. Boroyevich, R. Burgos *et al*., "Inverse Nyquist stability criterion for grid-tied inverters," *IEEE Transactions on Power Electronics*, vol. 32, no. 2, pp. 1548-1556, Feb. 2017.
[74] W. Cao, Y. Ma, and F. Wang, "Sequence-impedance-based harmonic stability analysis and controller parameter design of three-phase inverter-based multibus AC power systems," *IEEE Transactions on Power Electronics*, vol. 32, no. 10, pp. 7674-7693, Oct. 2017.
[75] W. Wu, Y. Chen, L. Zhou *et al*., "Sequence impedance modeling and stability comparative analysis of voltage-controlled VSGs and current-controlled VSGs," *IEEE Transactions on Industrial Electronics*, vol. 66, no. 8, pp. 6460-6472, Aug. 2019.
[76] W. Cao, Y. Ma, L. Yang *et al*., "*D-Q* impedance based stability analysis and parameter design of three-phase inverter-based AC power systems," *IEEE Transactions on Industrial Electronics*, vol. 64, no. 7, pp. 6017-6028, Jul. 2017.
[77] Z. Liu, J. Liu, W. Bao *et al*., "Infinity-norm of impedance-based stability criterion for three-phase AC distributed power systems with constant power loads," *IEEE Transactions on Power Electronics*, vol. 30, no. 6, pp. 3030-3043, Jun. 2015.
[78] B. Wen, D. Boroyevich, R. Burgos *et al*., "Small-signal stability analysis of three-phase AC systems in the presence of constant power loads based on measured *d-q* frame impedances," *IEEE Transactions on Power Electronics*, vol. 30, no. 10, pp. 5952-5963, Oct. 2015.
[79] S. Wang, Z. Liu, J. Liu *et al*., "Small-signal modeling and stability prediction of parallel droop-controlled inverters based on terminal characteristics of individual inverters," *IEEE Transactions on Power Electronics*, vol. 35, no. 1, pp. 1045-1063, Jan. 2020.
[80] W. Cao, Y. Ma, F. Wang *et al*., "Low-frequency stability analysis of inverter-based islanded multiple-bus AC microgrids based on terminal characteristics," *IEEE Transactions on Smart Grid*, vol. 11, no. 5, pp. 3662-3676, Sept. 2020.
[81] X. Hou, Y. Sun, X. Zhang *et al*., "Improvement of frequency regulation in VSG-based AC microgrid via adaptive virtual inertia," *IEEE Transactions on Power Electronics*, vol. 35, no. 2, pp. 1589-1602, Feb. 2020.
[82] J. Alipoor, Y. Miura, and T. Ise, "Power system stabilization using virtual synchronous generator with alternating moment of inertia," *IEEE Journal of Emerging and Selected Topics in Power Electronics*, vol. 3, no. 2, pp. 451-458, Jun. 2015.
[83] X. Hou, H. Han, C. Zhong *et al*., "Improvement of transient stability in inverter-based AC microgrid via adaptive virtual inertia," in *Proceedings of 2016 IEEE Energy Conversion Congress and Exposition (ECCE)*, Milwaukee, USA, Sept. 2016, pp. 1-6.
[84] H. Wu and X. Wang, "A mode-adaptive power-angle control method for transient stability enhancement of virtual synchronous generators," *IEEE Journal of Emerging and Selected Topics in Power Electronics*, vol. 8, no. 2, pp. 1034-1049, Jun. 2020.
[85] Z. Lan, D. Gan, L. Shi *et al*., "A study on the control of ac/dc power systems based on system dynamic COI," in *Proceedings of 2007 IEEE Power Engineering Society General Meeting*, Tampa, USA, Jun. 2007, pp. 1-5.
[86] J. Alipoor, Y. Miura, and T. Ise, "Stability assessment and optimization methods for microgrid with multiple VSG units," *IEEE Transactions on Smart Grid*, vol. 9, no. 2, pp. 1462-1471, Mar. 2018.
[87] M. Choopani, S. H. Hosseinain, and B. Vahidi, "A novel comprehensive method to enhance stability of multi-VSG grids," *International Journal of Electrical Power & Energy Systems*, vol. 104, pp. 502-514, Jan. 2019
[88] M. Choopani, S. H. Hosseinian, and B. Vahidi, "New transient stability and LVRT improvement of multi-VSG grids using the frequency of the center of inertia," *IEEE Transactions on Power Systems*, vol. 35, no. 1, pp. 527-538, Jan. 2020.
[89] K. M. Cheema and K. Mehmood, "Improved virtual synchronous generator control to analyse and enhance the transient stability of microgrid," *IET Renewable Power Generation*, vol. 14, no. 4, pp. 495-505, Nov. 2019.
[90] J. Chen, F. Prystupczuk, and T. O'Donnell, "Use of voltage limits for current limitations in grid-forming converters," *CSEE Journal of Power and Energy Systems*, vol. 6, no. 2, pp. 259-269, Jun. 2020.
[91] K. O. Oureilidis and C. S. Demoulias, "A fault clearing method in converter-dominated microgrids with conventional protection means," *IEEE Transactions on Power Electronics*, vol. 31, no. 6, pp. 4628-4640, Jun. 2016.
[92] E. Afshari, G. R. Moradi, R. Rahimi *et al*., "Control strategy for three-phase grid-connected PV inverters enabling current limitation under unbalanced faults," *IEEE Transactions on Industrial Electronics*, vol. 64, no. 11, pp. 8908-8918, Nov. 2017.
[93] L. Huang, H. Xin, Z. Wang *et al*., "Transient stability analysis and control design of droop-controlled voltage source converters considering current limitation," *IEEE Transactions on Smart Grid*, vol. 10, no. 1, pp. 578-591, Jan. 2019.
[94] W. Fan, X. Yan, and T. Hua, "Adaptive parameter control strategy of VSG for improving system transient stability," in *Proceedings of 2017 IEEE 3rd International Future Energy Electronics Conference and ECCE Asia (IFEEC 2017-ECCE Asia)*, Kaohsiung, China, Jun. 2017, pp. 2053-2058.
[95] H. Bevrani, T. Ise, and Y. Miura, "Virtual synchronous generators: a survey and new perspectives," *International Journal of Electrical Power & Energy Systems*, vol. 54, pp. 244-254, Jan. 2014.
[96] J. A. Suul, S. D'Arco, and G. Guidi, "Virtual synchronous machine-based control of a single-phase bi-directional battery charger for providing vehicle-to-grid services," *IEEE Transactions on Industry Applications*, vol. 52, no. 4, pp. 3234-3244, Jul.-Aug. 2016.
[97] K. Dhingra and M. Singh, "Frequency support in a micro-grid using virtual synchronous generator based charging station," *IET Renewable Power Generation*, vol. 12, no. 9, pp. 1034-1044, Jun. 2018.
[98] Y. Shi, W. Wu, H. Wang *et al*., "The parallel multi-inverter system based on the voltage-type droop control method," *IEEE Journal of Emerging and Selected Topics in Power Electronics*, vol. 4, no. 4, pp. 1332-1341, Dec. 2016.
[99] H. Zhang, S. Kim, Q. Sun *et al*., "Distributed adaptive virtual impedance control for accurate reactive power sharing based on consensus control in microgrids," *IEEE Transactions on Smart Grid*, vol. 8, no. 4, pp. 1749-1761, Jul. 2017.
[100] Q. Zhong, "Robust droop controller for accurate proportional load sharing among inverters operated in parallel," *IEEE Transactions on Industrial Electronics*, vol. 60, no. 4, pp. 1281-1290, Apr. 2013.
[101] H. Mahmood, D. Michaelson, and J. Jiang, "Accurate reactive power sharing in an islanded microgrid using adaptive virtual impedances," *IEEE Transactions on Power Electronics*, vol. 30, no. 3, pp. 1605-1617, Mar. 2015.
[102] L. Lin, H. Ma, and Z. Bai, "An improved proportional load-sharing strategy for meshed parallel inverters system with complex impedances," *IEEE Transactions on Power Electronics*, vol. 32, no. 9, pp. 7338-7351, Sept. 2017.
[103] K. Ahmed, M. Seyedmahmoudian, S. Mekhilef *et al*., "A review on primary and secondary controls of inverter-interfaced microgrid," *Journal of Modern Power Systems and Clean Energy*, vol. 9, no. 5, pp. 969-985, Sept. 2021.
[104] W. Yao, M. Chen, J. Matas *et al*., "Design and analysis of the droop control method for parallel inverters considering the impact of the complex impedance on the power sharing," *IEEE Transactions on Industrial Electronics*, vol. 58, no. 2, pp. 576-588, Feb. 2011.
[105] A. Haddadi and G. Joos, "Load sharing of autonomous distribution-level microgrids," in *Proceedings of 2011 IEEE Power and Energy Society General Meeting (PESGM)*, Detroit, USA, Jul. 2011, pp. 1-9.
[106] Y. W. Li and C. Kao, "An accurate power control strategy for power-electronics-interfaced distributed generation units operating in a low-voltage multibus microgrid," *IEEE Transactions on Power Electronics*, vol. 24, no. 12, pp. 2977-2988, Dec. 2009.
[107] T. Wen, X. Zou, D. Zhu *et al*., "Comprehensive perspective on virtual inductor for improved power decoupling of virtual synchronous generator control," *IET Renewable Power Generation*, vol. 14, no. 4, pp. 485-494, Nov. 2019.
[108] R. Wai, Q. Zhang, and Y. Wang, "A novel voltage stabilization and power sharing control method based on virtual complex impedance for an off-grid microgrid," *IEEE Transactions on Power Electronics*, vol. 34, no. 2, pp. 1863-1880, Feb. 2019.
[109] J. Chen, D. Yue, C. Dou *et al*., "A virtual complex impedance based P-V droop method for parallel-connected inverters in low-voltage AC microgrids," *IEEE Transactions on Industrial Informatics*, vol. 17, no. 3, pp. 1763-1773, Mar. 2021.
[110] P. Zhang, H. Zhao, H. Cai *et al*., "Power decoupling strategy based on 'virtual negative resistor' for inverters in low-voltage microgrids," *IET Power Electronics*, vol. 9, no. 5, pp. 1037-1044, Apr. 2016.
[111] S. M. Muyeen, R. Takahashi, and J. Tamura, "Operation and control of HVDC-connected offshore wind farm," *IEEE Transactions on Sustainable Energy*, vol. 1, no. 1, pp. 30-37, Apr. 2010.

[112] L. Zhang, L. Harnefors, and P. Mitra, "Offshore wind integration to a weak grid by VSC-HVDC links using power-synchronization control: a case study," in *Proceedings of 2014 IEEE PES General Meeting|Conference & Exposition*, National Harbor, USA, Jul. 2014, pp. 1-10.
[113] L. Huang, H. Xin, W. Zhen *et al*., "A virtual synchronous control for voltage-source converters utilizing dynamics of DC-link capacitor to realize self-synchronization," *IEEE Journal of Emerging and Selected Topics in Power Electronics*, vol. 5, no. 4, pp. 1565-1577, Dec. 2017.
[114] O. D. Adeuyi, M. Cheah-Mane, J. Liang *et al*., "Fast frequency response from offshore multiterminal VSC-HVDC schemes," *IEEE Transactions on Power Delivery*, vol. 32, no. 6, pp. 2442-2452, Dec. 2017.
[115] I. Cvetkovic, D. Boroyevich, R. Burgos *et al*., "Modeling and control of grid-connected voltage-source converters emulating isotropic and anisotropic synchronous machines," in *Proceedings of 2015 IEEE 16th Workshop on Control and Modeling for Power Electronics (COMPEL)*, Vancouver, Canada, Jul. 2015, pp. 1-5.
[116] F. Milano, F. Dörfler, G. Hug *et al*., "Foundations and challenges of low-inertia systems (invited paper)," in *Proceedings of 2018 Power Systems Computation Conference (PSCC)*, Dublin, Ireland, Jun. 2018, pp. 1-25.
[117] I. Cvetkovic, D. Boroyevich, R. Burgos *et al*., "Modeling of a virtual synchronous machine-based grid-interface converter for renewable energy systems integration," in *Proceedings of 2014 IEEE 15th Workshop on Control and Modeling for Power Electronics (COMPEL)*, Santander, Spain, Jun. 2014, pp. 1-7.
[118] T. Neumann, I, Erlich, B. Paz *et al*., "Novel direct voltage control by wind turbines," in *Proceedings of 2016 IEEE Power and Energy Society General Meeting (PESGM)*, Boston, USA, Jul. 2016, pp. 1-5.
[119] I. Erlich, A. Korai, T. Neumann *et al*., "New control of wind turbines ensuring stable and secure operation following islanding of wind farms," *IEEE Transactions on Energy Conversion*, vol. 32, no. 3, pp. 1263-1271, Sept. 2017.
[120] I. Erlich, A. Korai, and F. Shewarega, "Study on the minimum share of conventional generation units required for stable operation of future converter-dominated grids," in *Proceedings of 2018 IEEE Power & Energy Society General Meeting (PESGM)*, Portland, USA, Aug. 2018, pp. 1-5.
[121] L. Shi, G. P. Adam, R. Li *et al*., "Enhanced control of offshore wind farms connected to mtdc network using partially selective dc fault protection," *IEEE Journal of Emerging and Selected Topics in Power Electronics*, vol. 9, no. 3, pp. 2926-2935, Jun. 2021.
[122] S. Seman, R. Zurowski, and C. Taratoris "Interconnection of advanced type 4 WTGs with diode rectifier based HVDC solution and weak AC grids," in *Proceedings of the 14th Wind Integration Workshop*, Bruxelles, Belgium, Oct. 2015, pp. 1-6.
[123] R. Blasco-Gimenez, S. Añó -Villalba, J. Rodríguez-D'Derlée *et al*., "Distributed voltage and frequency control of offshore wind farms connected with a diode-based HVDC link," *IEEE Transactions on Power Electronics*, vol. 25, no. 12, pp. 3095-3105, Dec. 2010.
[124] L. Yu, R. Li, and L. Xu, "Distributed PLL-based control of offshore wind turbines connected with diode-rectifier-based HVDC systems," *IEEE Transactions on Power Delivery*, vol. 33, no. 3, pp. 1328-1336, June. 2018.
[125] M. H. Othman, H, Mokhlis, M. Mubin *et al*., "Progress in control and coordination of energy storage system-based VSG: a review," *IET Renewable Power Generation*, vol. 14, no. 2, pp. 177-187, Dec. 2019.
[126] J. Fang, Y. Tang, H. Li *et al*., "A battery/ultracapacitor hybrid energy storage system for implementing the power management of virtual synchronous generators," *IEEE Transactions on Power Electronics*, vol. 33, no. 4, pp. 2820-2824, Apr. 2018.
[127] X. Quan, R. Yu, X. Zhao *et al*., "Photovoltaic synchronous generator: architecture and control strategy for a grid-forming PV energy system," *IEEE Journal of Emerging and Selected Topics in Power Electronics*, vol. 8, no. 2, pp. 936-948, Jun. 2020.
[128] T. Patel, S. Brahma, J. Hernandez-Alvidrez *et al*., "Adaptive protection scheme for a real-world microgrid with 100% inverter-based resources," in *Proceedings of 2020 IEEE Kansas Power and Energy Confrence (KPEC)*, Manhattan, USA, Jul. 2020, pp. 1-6.
[129] A. Haddadi, M. Zhao, I. Kocar *et al*., "Impact of inverter-based resources on negative sequence quantities-based protection elements," *IEEE Transactions on Power Delivery*, vol. 36, no. 1, pp. 289-298, Feb. 2021.
[130] Y. Fang, K. Jia, Z. Yang *et al.*, "Impact of inverter-interfaced renewable energy generators on distance protection and an improved scheme," *IEEE Transactions on Power Electronics*, vol. 66, no. 9, pp. 7078-7088, Sept. 2019.
[131] W. T. El-Sayed, E. F. El-Saadany, and H. H. Zeineldin, "Interharmonic differential relay with a soft current limiter for the protection of inverter-based islanded microgrids," *IEEE Transactions on Power Delivery*, vol. 36, no. 3, pp. 1349-1359, Jun. 2021.
[132] K. Saleh, M. A. Allam, and A. Mehrizi-Sani, "Protection of inverter-based islanded microgrids via synthetic harmonic current pattern injection," *IEEE Transactions on Power Delivery*, vol. 36, no. 4, pp. 2434-2445, Aug. 2021.

Haobo Zhang received the B.E. degree in electrical engineering from Huazhong University of Science and Technology (HUST), Wuhan, China, in 2020, where he is currently working toward the M.E. degree. His research interests include protection and control of modular multilevel converter based high-voltage direct current (MMC-HVDC) and DC grids.

Wang Xiang received the B.Eng. and Ph.D. degrees both in electrical engineering from Huazhong University of Science and Technology (HUST), Wuhan, China, in 2012 and 2017, respectively. He was a Visiting Ph.D. student at the University of Aberdeen, Aberdeen, UK, and the University of Strathclyde, Glasgow, UK, in 2014 and 2016, respectively. He joined the University of Strathclyde, Glasgow, UK, in 2018, and is currently a Research Associate. His main research interests include MMC-HVDC, high power DC/DC converters and DC grids.

Weixing Lin obtained his B.E. and Ph.D. degrees in electrical engineering from Huazhong University of Science and Technology (HUST), Wuhan, China, in 2008 and 2014 respectively. He was the director of High-voltage Direct Current (HVDC) Department at TBEA China Xinjiang Sunoasis Co. Ltd, Ürümqi, China. He is currently with Huazhong University of Science and Technology. His research interests lie in HVDC, MMC, DC-DC autotransformer, and DC grid.

Jinyu Wen received his B.Eng. and Ph.D. degrees all in electrical engineering from Huazhong University of Science and Technology (HUST), Wuhan, China, in 1992 and 1998, respectively. He was a Visiting Student from 1996 to 1997 and Research Fellow from 2002 to 2003 all at the University of Liverpool, Liverpool, UK, and a Senior Visiting Researcher at the University of Texas at Arlington, Arlington, USA, in 2010. From 1998 to 2002, he was a Director Engineer in XJ Electric Co. Ltd., Xuchang, China. In 2003, he joined the HUST and now is a Professor at HUST. His current research interests include renewable energy integration, energy storage application, DC grid, and power system operation and control.